Inorganic Chemistry

Article

pubs.acs.org/IC

Synthesis, Structural Elucidation, and Catalytic Properties in Olefin Epoxidation of the Polymeric Hybrid Material $[Mo_3O_9(2\text{-}[3(5)\text{-}Pyrazolyl]pyridine)]_n$

Tatiana R. Amarante,[†] Patrícia Neves,[†] Ana C. Gomes,[†] Mariela M. Nolasco,[†] Paulo Ribeiro-Claro,[†] Ana C. Coelho,[†] Anabela A. Valente,[†] Filipe A. Almeida Paz,*[,†] Stef Smeets,[‡] Lynne B. McCusker,[‡] Martyn Pillinger,[†] and Isabel S. Gonçalves*[,†]

[†]Department of Chemistry, CICECO, University of Aveiro, Campus Universitário de Santiago, 3810-193 Aveiro, Portugal

[‡]Laboratory of Crystallography, ETH Zürich, CH-8093, Zürich, Switzerland

Supporting Information

ABSTRACT: The reaction of $[MoO_2Cl_2(pzpy)]$ (**1**) (pzpy = 2-[3(5)-pyrazolyl]pyridine) with water in an open reflux system (16 h), in a microwave synthesis system (120 °C, 2 h), or in a Teflon-lined stainless steel digestion bomb (100 °C, 19 h) gave the molybdenum oxide/pyrazolylpyridine polymeric hybrid material $[Mo_3O_9(pzpy)]_n$ (**2**) as a microcrystalline powder in yields of 72−79%. Compound **2** can also be obtained by the hydrothermal reaction of MoO_3, pzpy, and H_2O at 160 °C for 3 d. Secondary products isolated from the reaction solutions included the salt $(pzpyH)_2(MoCl_4)$ (**3**) (pzpyH = 2-[3(5)-pyrazolyl]pyridinium), containing a very rare example of the tetrahedral $MoCl_4^{2-}$ anion, and the tetranuclear compound $[Mo_4O_{12}(pzpy)_4]$ (**4**). Reaction of **2** with excess *tert*-butylhydroperoxide (TBHP) led to the isolation of the oxodiperoxo complex $[MoO(O_2)_2(pzpy)]$ (**5**). Single-crystal X-ray structures of **3** and **5** are described. Fourier transform (FT)-IR and FT Raman spectra for **1**, **4**, and **5** were assigned based on density functional theory calculations. The structure of **2** was determined from synchrotron powder X-ray diffraction data in combination with other physicochemical information. In **2**, a hybrid organic−inorganic one-dimensional (1D) polymer, $^1_\infty[Mo_3O_9(pzpy)]$, is formed by the connection of two very distinct components: a double ladder-type inorganic core reminiscent of the crystal structure of MoO_3 and 1D chains of corner-sharing distorted $\{MoO_4N_2\}$ octahedra. Compound **2** exhibits moderate activity and high selectivity when used as a (pre)catalyst for the epoxidation of *cis*-cyclooctene with TBHP. Under the reaction conditions used, **2** is poorly soluble and is gradually converted into **5**, which is at least partly responsible for the catalytic reaction.

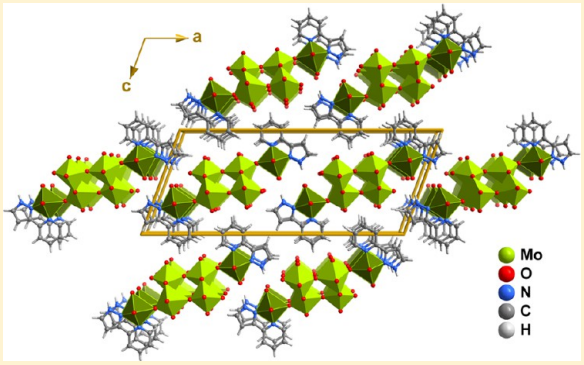

INTRODUCTION

Among the various oxyhalides of molybdenum, dichlorodioxomolybdenum(VI), MoO_2Cl_2, has received much attention as a starting material for preparing numerous molybdenum compounds and as a catalyst in organic transformations.[1] Most of the synthetic chemistry has dealt with the synthesis of adducts with the general formula $[MoO_2Cl_2(L)_n]$, where L is a mono- (n = 2) or bidentate (n = 1) ligand such as a nitrogen or oxygen-donating solvent molecule (e.g., tetrahydrofuran, dimethylsulfoxide, dimethylformamide, acetonitrile),[2] 2,2′-bipyridines,[3] phosphine oxides,[4] thio- and seleno-ethers.[5] The stability of these compounds toward moisture varies from quite stable in the case of the bipyridine adducts to extremely sensitive in the case of the thio- and seleno-ether complexes. Even for the most stable complexes the Mo−Cl bond is susceptible to hydrolysis. Thus, in the presence of residual or small amounts of water, $[MoO_2Cl_2(L)_n]$ complexes have been shown to dimerize, leading to the isolation of dioxo(μ-oxo)molybdenum(VI) complexes with the general formula $[Mo_2O_4(\mu_2\text{-}O)Cl_2(L)_n]$.[2c,6] Several higher nuclearity oxomolybdenum(VI) compounds have been isolated after the reaction of dichlorodioxomolybdenum(VI) complexes with excess water, namely the hexamolybdate isopolyanion in $[(H_3O)(18\text{-crown-}6)]_2[Mo_6O_{19}]$ (L = H_2O in the precursor complex),[7] the octanuclear complex $[Mo_8O_{22}(OH)_4(di\text{-}tBu\text{-}bipy)_4]$ (di-*t*Bu-bipy = 4,4′-di-*tert*-butyl-2,2′-bipyridine),[8] and the polymeric materials $\{[MoO_3(bipy)][MoO_3(H_2O)]\}_n$[9] (bipy = 2,2′-bipyridine) and $[Mo_2O_6(HpypzA)]$ (HpypzA = [3-(pyridinium-2-yl)-1*H*-pyrazol-1-yl]acetate).[10] The hydrolysis and condensation of dichlorodioxomolybdenum(VI) complexes is therefore an interesting, yet still largely unexplored, pathway toward molybdenum oxide-based organic−inorganic hybrid materials, which are of interest due to their potential application

Received: December 10, 2013
Published: February 12, 2014

   dx.doi.org/10.1021/ic403033j | *Inorg. Chem.* 2014, 53, 2652−2665

Scheme 1. Synthesis of Compounds 2−5 Starting from the Dioxomolybdenum(VI) Complex 1[a]

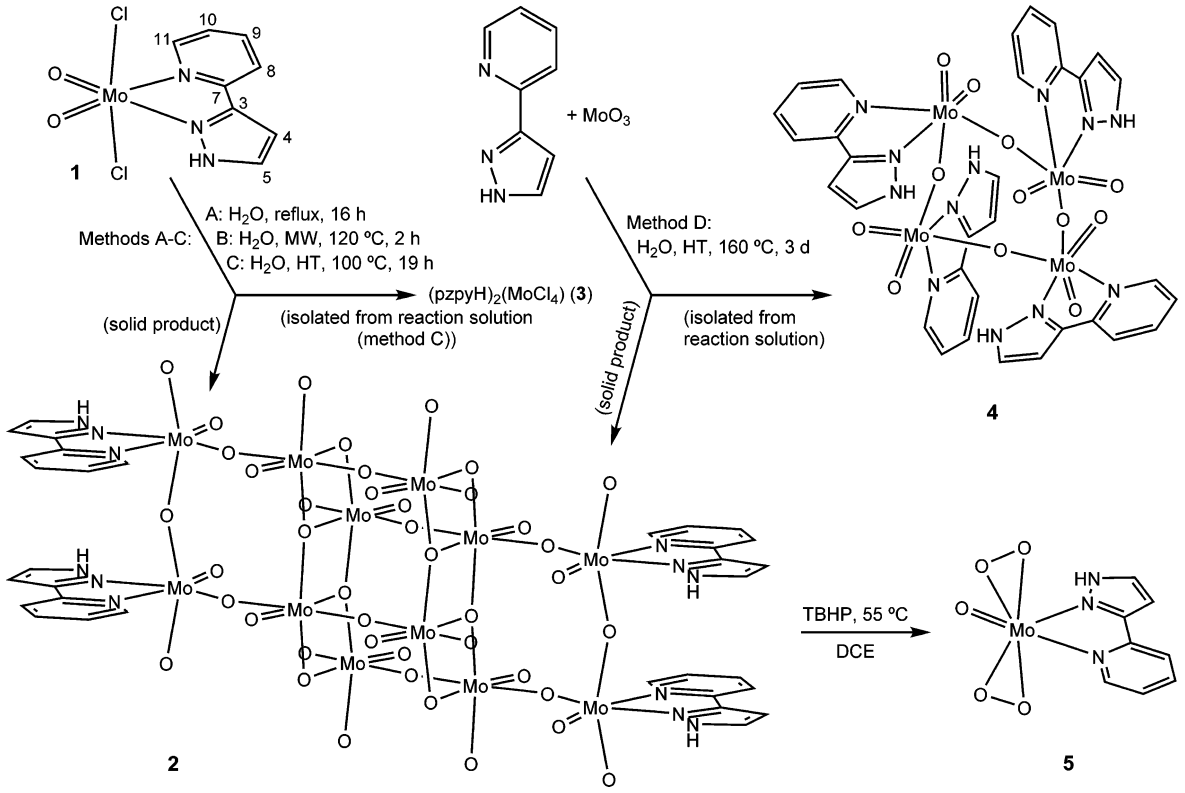

[a]MW = microwave, HT = hydrothermal.

in important fields such as catalysis, sorption, electrical conductivity, magnetism, electronics, and optical materials.[8−11]

In the present Work we set out to extend the structural diversity of molybdenum oxide-based hybrid materials by studying the hydrolysis of the complex $[MoO_2Cl_2(pzpy)]$ (**1**) (pzpy = 2-[3(5)-pyrazolyl]pyridine). Hybrid materials containing pyrazolylpyridines are of interest since these ligands are known to lead to very effective molecular Mo^{VI} catalysts for olefin epoxidation.[6c,12] Usually, these ligands are *N,N*-chelated to the Mo^{VI} center. However, in our previous study of the hydrolysis of the complex $[MoO_2Cl_2(pypzEA)]$ (pypzEA = ethyl[3-(pyridin-2-yl)-1*H*-pyrazol-1-yl]acetate), the coordination mode of the pyrazolylpyridine ligand switched from *N,N*-bidentate in the precursor to syn, syn *O,O*-bidentate in the molybdenum oxide/pyrazolylpyridine composite material $[Mo_2O_6(HpypzA)]$ (due to concomitant hydrolysis of the ester group in the precursor).[10] Hence, we were led to examine the hydrolysis of a dichlorodioxomolybdenum(VI) complex containing the simplest pyrazolylpyridine ligand, namely, pzpy. The treatment of the dichloro complex **1** with water under hydrothermal, open reflux, or microwave-assisted heating conditions leads to the isolation of the inorganic/organic polymeric composite oxide $[Mo_3O_9(pzpy)]_n$ (**2**), the structure of which has been determined through synchrotron powder X-ray diffraction in conjunction with other characterization data. Material **2** has also been isolated by the hydrothermal treatment of an aqueous solution containing MoO_3 and pzpy. The molybdenum-catalyzed epoxidation of *cis*-cyclooctene was chosen as a model reaction to assess the catalytic properties of **2**.

EXPERIMENTAL SECTION

Materials and Methods. MoO_3 (99.5%, AnalaR), *cis*-cyclooctene (Cy, 95%), 5−6 M *tert*-butylhydroperoxide (TBHP) in decane, acetone (99.5%), pentane (99%), diethyl ether (99.8%), anhydrous *α,α,α*-trifluorotoluene (TFT, 99%), 1,2-dichloroethane (DCE, 99%), *N,N*-dimethylformamide (99%), and undecane (99%) were acquired from Sigma-Aldrich unless otherwise stated. For catalysis, DCE was dried prior to use by stirring over CaH_2 overnight, followed by distillation and storage over activated 4 Å molecular sieves. The TBHP solution was dried prior to use using activated 3 Å molecular sieves. The ligand pzpy[13] and the complex $[MoO_2Cl_2(pzpy)]$ (**1**)[6c] were prepared by using literature procedures.

Elemental analysis for C, H, and N was performed at the University of Aveiro using a Truspec instrument. Mo was determined by inductively coupled plasma−optical emission spectroscopy at C.A.C.T.I., University of Vigo, Spain. Routine powder X-ray diffraction (PXRD) data were collected at room temperature on a Philips X'Pert MPD diffractometer (Cu Kα X-radiation, λ = 1.54060 Å) fitted with a curved graphite monochromator and a flat plate sample holder, in a Bragg−Brentano para-focusing optics configuration (40 kV, 50 mA). Samples were step-scanned in 0.02° 2θ steps with a counting time of 30 s per step. Scanning electron microscopy (SEM) images and energy dispersive X-ray spectroscopy (EDS) data were collected using a Hitachi SU-70 microscope operating at 15 kV. Samples were prepared by deposition on aluminum sample holders followed by carbon coating, using an Emitech K 950 carbon evaporator.

The room-temperature Fourier transform (FT)-Raman spectra in the 150−3500 cm^{-1} range were recorded with 2 cm^{-1} resolution on an RFS-100 Bruker FT-spectrometer, using a Nd:YAG laser (Coherent Compass-1064/500) with an excitation wavelength of 1064 nm. Room-temperature FT-IR spectra were recorded with a Mattson 7000 spectrometer, using a globar source, a deuterated triglycine sulfate detector, and potassium bromide cells, with 2 cm^{-1} resolution and triangular apodization. Attenuated total reflectance (ATR) FT-IR spectra were measured on a Bruker optics Tensor 27 equipped with a

dx.doi.org/10.1021/ic403033j | Inorg. Chem. 2014, 53, 2652−2665

Specac Golden Gate Mk II ATR accessory having a diamond top plate and KRS-5 focusing lenses. ^{1}H solution NMR spectra were obtained at 300.13 MHz with a Bruker Avance 300 spectrometer using $(CD_3)_2SO$ as solvent. Chemical shifts are quoted in ppm from tetramethylsilane (TMS). Solid-state $^{13}C\{^1H\}$ cross-polarization (CP) magic-angle-spinning (MAS) NMR spectra were recorded using a Bruker Avance 500 (narrow bore) spectrometer with an ultrashielded static magnetic field of 125.76 MHz. The spectra were recorded with 3.5 μs ^{1}H 90° pulses, 1.5 ms contact time, spinning rate of 9 kHz, and 5 s recycle delays. Chemical shifts are quoted in ppm from TMS.

The microwave-assisted synthesis was carried out in a Discover S-Class (CEM Corporation, USA) microwave oven at 2.45 GHz, using a glass vessel with a capacity of 35 mL, under stirring and simultaneous cooling with compressed air (15 psi) to prevent bulk heating. A dynamic method was used in which the power was automatically controlled based on the temperature feedback measured using a vertically focused IR sensor.

Synthesis of $[Mo_3O_9(pzpy)]_n$ (2). *Method A.* A mixture of complex **1** (0.50 g, 1.45 mmol) and distilled water (20 mL) was refluxed in a Schlenk tube for 16 h under nitrogen. The resultant blue precipitate was separated from the colorless solution (pH 1−3) by filtration, washed with water (2 × 10 mL), acetone (2 × 10 mL), and diethyl ether (2 × 10 mL), vacuum-dried, and identified as **2** (0.22 g, 79%; based on Mo) by elemental analysis, FT-IR spectroscopy, and PXRD.

Method B. A mixture of **1** (0.10 g, 0.29 mmol) and water (20 mL) was stirred and heated to 120 °C inside a microwave oven and maintained at this temperature for 2 h. The resultant blue solid was separated from the colorless mother liquor (pH 1−3) by filtration, washed with water (2 × 10 mL), acetone (2 × 10 mL), and diethyl ether (2 × 10 mL), vacuum-dried, and identified as **2** (0.04 g, 72%; based on Mo) by elemental analysis, FT-IR spectroscopy, and PXRD.

Method C. A Teflon-lined stainless-steel autoclave was charged with **1** (0.24 g, 0.70 mmol) and water (15 mL) and heated in an oven at 100 °C for 19 h. The resultant blue solid was separated from the aqueous mother liquor by filtration, washed with acetone (6 mL), vacuum-dried, and identified as **2** (0.10 g, 74%; based on Mo) by elemental analysis, FT-IR spectroscopy, and PXRD. After concentrating the filtrate under reduced pressure, small crystals were obtained, which were identified by single-crystal X-ray diffraction as the salt $(pzpyH)_2(MoCl_4)$ (**3**), where pzpyH stands for 2-[3(5)-pyrazolyl]-pyridinium (please see the Supporting Information for full details of the structural elucidation).

Method D. A Teflon-lined stainless steel autoclave with a capacity of 25 mL was charged with MoO_3 (0.14 g, 0.97 mmol), the ligand pzpy (0.14 g, 0.97 mmol), and water (10 mL) and heated in an oven at 160 °C for 3 d. The resultant pale-blue solid was separated from the pale-yellow mother liquor by filtration, washed with diethyl ether (4 × 20 mL), and vacuum-dried. Yield: 0.054 g, 29% (based on Mo). Anal. Calcd for $C_8H_7Mo_3N_3O_9$ (576.98): C, 16.65; H, 1.22; N, 7.28; Mo, 49.9. Found: C, 16.65; H, 1.23; N, 7.10; Mo, 51.8%. Selected FT-IR (KBr, cm^{-1}): ν = 316w, 352m, 399m, 420w, 535vs, 672vs, 698s, 748s, 847vs, 911w, 930s, 935s, 941s, 967vs, 1021m, 1064m, 1096m, 1151m, 1219m, 1261m, 1295m, 1369m, 1385sh, 1433m, 1455m, 1472m, 1519m, 1570m, 1610s, 2827w, 2919sh, 2963w, 3025w, 3050vw, 3081sh, 3115vw, 3128m, 3142m. Selected FT-Raman (cm^{-1}): ν = 159m, 184m, 193m, 214m, 231m, 245w, 271m, 288w, 298w, 316m, 343m, 384w, 394w, 611w, 667s, 698m, 711sh, 744vw, 848vs, 926m, 946m, 977m, 1021w, 1052w, 1097vw, 1149vw, 1313m, 1369w, 1455w, 1472w, 1518sh, 1539w, 1570w, 1607m, 3067m, 3074sh, 3092m, 3129m, 3142m. ^{1}H NMR (300.13 MHz, 25 °C, DMSO-d_6): δ = 13.05 (br, NH), 8.64 (d, 1H, H11), 8.1−7.8 (series of overlapping broad peaks and multiplets, 3H, H5,8,9), 7.37 (t, 1H, H10), 6.90 (d, 1H, H4) ppm (please see Scheme 1 for atom numbering). $^{13}C\{^1H\}$ CP MAS NMR: δ = 99.7 (C4), 120.6 (C8), 125.6 (C10), 133.1 (C5/C9), 143.4 (C11), 145.8 (C3), 146.8 (C7) ppm.

The pale-yellow filtrate from the above reaction was concentrated, and acetone (5 mL) was added. After addition of diethyl ether (20 mL), a solid precipitated, which was washed with diethyl ether (3 × 20 mL), vacuum-dried, and identified as the tetranuclear compound $[Mo_4O_{12}(pzpy)_4]$ (**4**) (0.05 g, 18%) by a comparison of the experimental PXRD pattern with a simulated one calculated from the structural data reported by Li et al.[14] FT-IR, NMR, and elemental analysis data were in agreement with published results.[12e] Selected FT-IR (KBr, cm^{-1}): ν = 343m, 376m, 402s, 436m, 489vw, 645m, 692w, 710w, 778s, 798sh, 818s, 849s, 922w, 936w, 975w, 1024w, 1053sh, 1064m, 1093m, 1152m, 1230m, 1255m, 1296m, 1314m, 1372s, 1383vs, 1430s, 1438s, 1448s, 1473m, 1522m, 1568m, 1608vs, 3114m, 3139m. Selected FT-Raman (cm^{-1}): ν = 137vs, 210m, 230w, 245w, 269m, 304w, 342m, 360w, 367w, 376w, 403m, 491w, 508w, 622vw, 643m, 696w, 709m, 794sh, 812m, 848vs, 900s, 908sh, 943w, 976m, 1022m, 1052m, 1063sh, 1088w, 1114vw, 1144m, 1255w, 1314m, 1370m, 1430sh, 1448w, 1473m, 1524s, 1567s, 1607vs, 3044m, 3060m, 3088m, 3114m, 3137m.

$[MoO(O_2)_2(pzpy)]$ (5). A mixture comprising **2** (0.10 g, 0.17 mmol), 5−6 M TBHP in decane (82.5 mmol), and DCE (30 mL) was heated at 55 °C for 24 h. After this time the reaction mixture was centrifuged, and then pentane and diethyl ether were added to the liquid phase, resulting in the precipitation of a pale-yellow solid (0.017 g, 10%), which was identified as the oxodiperoxo complex $[MoO(O_2)_2(pzpy)]$ (**5**)[12a] by elemental analysis, PXRD, FT-IR, and NMR spectroscopy. Crystals suitable for X-ray diffraction were obtained by slow diffusion of diethyl ether into a concentrated solution of **5** in DMF. The PXRD pattern of the bulk product **5** was in excellent agreement with a simulated pattern calculated from the single-crystal X-ray structural data (Figure S1 in the Supporting Information). Anal. Calcd for $C_8H_7MoN_3O_5$ (321.10): C, 29.92; H, 2.20; N, 13.09. Found: C, 29.75; H, 1.96; N 13.08%. Selected FT-IR (KBr, cm^{-1}): ν = 288m, 325m, 393m, 437w, 492m, 512s, 539m, 584s, 615m, 643m, 655s, 713w, 778vs, 864s (ν(O−O)), 875sh, 924m, 950vs (ν(Mo═O)), 983m, 1025m, 1051m, 1070m, 1100m, 1126m, 1157m, 1166sh, 1216m, 1227m, 1257m, 1304m, 1315sh, 1364m, 1437s, 1458m, 1479m, 1522m, 1542m, 1570m, 1610vs, 2825w, 2917s, 3010s, 3054m, 3092m, 3124m, 3135m (ν(NH)). Selected FT-Raman (cm^{-1}): ν = 155m, 187w, 240vw, 260m, 295m, 320w, 393m, 492w, 511m, 538m, 585m, 643m, 657sh, 714m, 862sh, 873s, 924m, 940vs, 955w, 982w, 1023m, 1052w, 1075vw, 1101w, 1126w, 1158m, 1165sh, 1218vw, 1230sh, 1257vw, 1311s, 1365m, 1438sh, 1458m, 1480m, 1522w, 1541s, 1570s, 1610vs, 3070s, 3091m, 3123m, 3139s. ^{1}H NMR (300.13 MHz, 25 °C, DMSO-d_6): δ = 13.05 (br, NH), 8.58 (d, 1H, H11), 7.95 (d, 1H, H8), 7.84 (t, 1H, H9), 7.76 (br s, 1H, H5), 7.31 (dd, 1H, H10), 6.84 (d, 1H, H4) ppm.

X-ray Diffraction Studies. A detailed description of the powder and single crystal X-ray diffraction studies is given in the Supporting Information.

DFT Calculations. DFT calculations were performed using the G03W program package,[15] running on a personal computer. Crystallographic data for **1**,[6c] **4**,[14] and **5** (this Work) were used as the starting point for the B3LYP full geometry optimizations using the standard LanL2DZ basis set and effective core potentials (performed for the isolated molecule and without symmetry constraints). Harmonic vibrational wavenumbers and IR/Raman intensities were calculated at the same level for all optimized structures, which were shown to have no negative eigenvalues for the Hessian matrices. To provide the best fit with experimental values, the harmonic vibrational wavenumbers were scaled by a factor of 0.961.[16] The vibrational assignments were based on the atomic displacements and calculated intensities.

Catalytic *cis*-Cyclooctene Epoxidation. Batch Reactions. Catalytic experiments were carried out under autogenous pressure in borosilicate reactors (5 mL) equipped with a magnetic stirring bar and a Teflon valve for sampling. The reactors were charged with compound **2** (method A) in an amount equivalent to 18 μmol of molybdenum, *cis*-cyclooctene (Cy, 1.8 mmol) and, optionally, cosolvent (1 mL). Subsequently, the reactors were immersed in an oil bath thermostatted at the desired reaction temperature (55 or 75 °C) and stirred at 1000 rpm during 10 min. In a similar fashion, the predried 5−6 M TBHP in decane (2.75 mmol) was preheated to obtain isothermal initial conditions since otherwise the initial heating-up period would be ca. 7 min.[9] The initial instant of the catalytic

dx.doi.org/10.1021/ic403033j | Inorg. Chem. 2014, 53, 2652−2665

reaction was taken to be the moment that the oxidant solution was added to the reactor. The reactions were carried out under air; molecular oxygen did not influence the catalytic reaction, ascertained by the fact that no reaction of Cy took place in the presence of **2** without TBHP.

The evolutions of the catalytic reactions were monitored via sampling throughout 24 h reaction. The samples were analyzed using a Varian 3900 GC equipped with a flame ionization detector and a capillary column (J&W Scientific DB-5, 30 m × 0.25 mm × 0.25 μm) using undecane as internal standard.

Catalyst Stability Tests. Compound **2** was not completely soluble in the reaction media for all conditions used. After each 24 h batch run the solid phase was separated from the liquid phase by centrifugation (3000 rpm), washed with pentane, and vacuum-dried at 55 °C for 1 h, giving the recovered solids mentioned throughout the discussion.

The homogeneous or heterogeneous nature of the catalytic reaction was checked by carrying out catalytic tests denoted CatFilt_Test. The reaction mixture was filtered at 2 h at the reaction temperature (75 °C), using a 0.2 μm poly(tetrafluoroethylene) (PTFE) membrane, and then the filtrate was transferred to a separate reactor (with preheated walls) containing a stirring bar and immersed in an oil bath thermostatted at the desired reaction temperature. The evolution of the catalytic reaction was monitored for 6 h, counting from the initial instant of the CatFilt_Test. The increment in conversion for the time interval between the instant of the filtration and 6 h reaction is denoted Δ*F*iltCat; this value was compared with Δnone for the same time interval, which corresponds to the increment in conversion for the reaction of Cy carried out in the absence of catalyst. The catalytic reaction may be considered heterogeneous when (Δ*F*iltCat)/(Δnone) = 1 (Δnone > 0), and a homogeneous catalytic contribution exists when (Δ*F*iltCat)/(Δnone) > 1.

In some cases the contribution of the dissolved metal species was checked by performing assays denoted Dissolv_Test, which consisted of the predissolution of **2** in the cosolvent/TBHP mixture during 24 h at 75 °C, prior to addition of the substrate. This test is particularly important considering that the initial dissolution of the metal species may be rate-limiting to the overall reaction system.[11e,17] After 24 h the biphasic solid−liquid mixture was filtered at the reaction temperature, using a 0.2 μm PTFE membrane. The filtrate was transferred to a separate reactor, which was immersed in an oil bath thermostatted at 75 °C. After stirring for 10 min, the olefin (also preheated) was added in an amount equivalent to the molar concentration of substrate used in a typical catalytic test. The evolutions of the homogeneous catalytic reactions were monitored throughout 24 h.

RESULTS AND DISCUSSION

Synthesis. The complex $[MoO_2Cl_2(pzpy)]$ (**1**) was prepared as described previously by the addition of 2-[3(5)-pyrazolyl]pyridine (pzpy) to a solution of $[MoO_2Cl_2(THF)_2]$ in THF.[6c] The reaction of **1** with water was carried out either in an open reflux system under nitrogen (16 h, oil bath heating, method A), in a sealed glass vessel with microwave-assisted heating (120 °C, 2 h, method B), or in a sealed Teflon-lined stainless-steel digestion bomb (autogenous pressure, 100 °C, 19 h, method C). In each case a pale blue solid suspended in an acidic solution (pH 1−3) was obtained, which was recovered by filtration, washed with water and organic solvents, and vacuum-dried. Practically identical elemental analysis, FT-IR, and PXRD data were obtained for all three solid products, indicating that the heating method had no significant influence on the outcome of the reaction (Figure S2 in the Supporting Information; different heating methods were employed in an effort to obtain higher yields and/or a more crystalline product). No Cl in the product was detected by EDS analyses. On the basis of the characterization data and the crystal structure solution described below, the product is formulated as $[Mo_3O_9(pzpy)]_n$ (**2**) (Scheme 1).

The yield of **2** was in the range of 72−79% for all three methods. In the case of method C, concentration of the filtrate led to the appearance of small crystals, which were identified by single-crystal X-ray diffraction as the salt $(pzpyH)_2(MoCl_4)$ (**3**) (please see the Supporting Information for full details of the structural elucidation). Compound **2** was also obtained in a yield of 29% by the reaction of MoO_3, pzpy, and H_2O in the mole ratio of 1:1:560 at 160 °C for 3 d in a Teflon-lined digestion bomb (method D). The pale-yellow filtrate from this reaction was concentrated, acetone/diethyl ether added, and the resultant precipitate identified as the tetranuclear compound $[Mo_4O_{12}(pzpy)_4]$ (**4**) (Scheme 1) by a comparison of the experimental PXRD pattern with a simulation based on the crystal structure data reported by Li et al.[14] Even though these authors obtained crystals of **4** by using the same hydrothermal method, they did not report the formation of an insoluble product (**2**). In previous studies, compound **4** was also obtained after (a) use of $[MoO_2(OSiPh_3)_2(pzpy)]$ as a (pre)catalyst in olefin epoxidation with TBHP[6c] and (b) oxidative decarbonylation of the tetracarbonyl complex *cis*-$[Mo(CO)_4(pzpy]$ with excess TBHP.[12e]

In an attempt to obtain a better understanding of the Mo-containing species formed during catalytic olefin epoxidation with compound **2** as the (pre)catalyst, the reaction of **2** in DCE with a large excess (ca. 150 equiv) of the oxidant TBHP was performed separately. After heating at 55 °C for 24 h, the reaction mixture was centrifuged, and pentane and diethyl ether were added to the liquid phase, resulting in the precipitation of a pale-yellow solid, which was identified as the oxodiperoxo complex $[MoO(O_2)_2(pzpy)]$ (**5**) (Scheme 1). Crystals suitable for X-ray diffraction were obtained by slow diffusion of diethyl ether into a concentrated solution of **5** in DMF.

Crystal Structure of 2. Regardless of the synthesis method (A−D), material **2** was systematically isolated as a microcrystalline powder. SEM studies for the material obtained using method C showed that the morphology consisted of very thin and long (hair-like) needles (Figure 1). A full structural

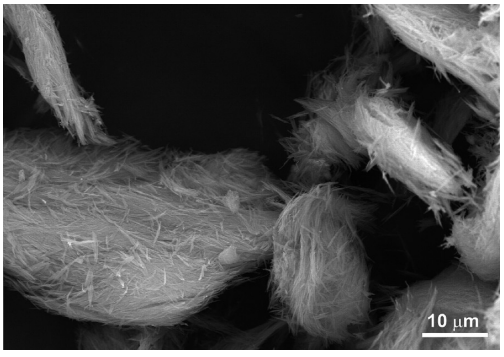

Figure 1. Representative SEM image of material **2** obtained by method C.

elucidation could only be achieved by using ab initio PXRD methods (Table 1) based on high-resolution synchrotron X-ray data (Figure 2) in combination with other relevant characterization techniques (please see the Supporting Information for experimental and structure refinement details). This tandem approach was used by some of us in the past to unveil the structural features of novel molybdenum oxide/organic hybrid materials such as $(DMA)[MoO_3(Hbpydc)]_n \cdot H_2O$ (where DMA^+ = dimethylammonium; H_2bpydc = 2,2′-bipyridine-

dx.doi.org/10.1021/ic403033j | Inorg. Chem. 2014, 53, 2652−2665

Table 1. X-ray Data Collection, Crystal Data, and Structure Refinement Details for $[Mo_3O_9(pzpy)]_n$ (2)

Data Collection	
diffractometer	I11 beamline—Diamond, U.K.
wavelength (Å)	0.82661(1)
temperature (K)	100
geometry	Debye–Scherrer
2θ range (deg)	2.500 to 50.000
step size (deg)	0.002
Unit Cell	
formula	$C_8H_7Mo_3N_3O_9$
formula weight	576.99
crystal system	monoclinic
space group	$C2/m$
a (Å)	30.2491(5)
b (Å)	3.72717(5)
c (Å)	12.8518(3)
γ (deg)	110.1955(16)
volume (Å^3)	1359.88(5)
Z	4
D_c (g cm^{-3})	2.818
Reliability Factors	
R_p	14.60
R_{wp}	16.22
R_{exp}	4.01
goodness-of-fit	4.05

5,5′-dicarboxylic acid)[11e] and $\{[MoO_3(bipy)]\text{-}[MoO_3(H_2O)]\}_n$.[9]

The crystal structure of $[Mo_3O_9(pzpy)]_n$ (**2**) is based on three crystallographically independent Mo^{VI} metal centers and one pzpy organic ligand. These four moieties are structurally located on special positions belonging to the mirror plane of the $C2/m$ monoclinic unit cell, alongside with 7 (of the 9) crystallographically independent oxygen atoms. The three single Mo^{VI} centers (Mo1, Mo2, and Mo3) have considerably distinct coordination environments as well as distinct structural functions in the crystal structure of **2** (Figure 3a,c–e). Only Mo1 has the organic ligand in its coordination environment in a typical *N,N*-chelate fashion, with the overall $\{MoN_2O_4\}$ coordination geometry resembling a distorted octahedron (Figure 3c): the Mo1–(N,O) distances range from 1.909(3) to 2.35(2) Å, and the cis and trans octahedral angles were found in the 66.8(10)–117.9(8)° and 146.5(9)–162.4(9)° ranges, respectively (Tables 2 and 3). The coordination spheres of Mo2 and Mo3 are uniquely composed of oxygen atoms, $\{MoO_6\}$ (Figures 3d and 3e), and exhibit very similar geometrical features: the Mo–O distances for the two metal environments were found in the 1.691(16)–2.325(18) Å range, and the cis and trans octahedral angles were in the 149.8(8)–179.5(8)° and 73.6(8)–104.3(7)° intervals, respectively (Tables 2 and 3).

From these data, it is difficult to properly evaluate and compare the degree of distortion for each Mo^{VI} octahedron: while the presence of pzpy in the coordination sphere of Mo1 seems to visually indicate a more distorted octahedron (Figure 3c), the values for the angles and distances are, on average, more spread out for Mo2 and Mo3. To further help in the evaluation of the variation of the degree of distortion of the Mo^{VI} octahedra, we decided to employ an adaptation of a simple method proposed by Baur[18] to calculate a distortion index (DI) for bonds and angles:

$$DI_{bond} = \frac{\sum_{i=1}^{n} \left| d(\text{Mo—(N, O)})_i - d(\text{Mo—(N, O)})_{average} \right|}{\sum_{i=1}^{n} \left| d(\text{Mo—(N, O)})_i \right|} \quad \text{(Equation 1)}$$

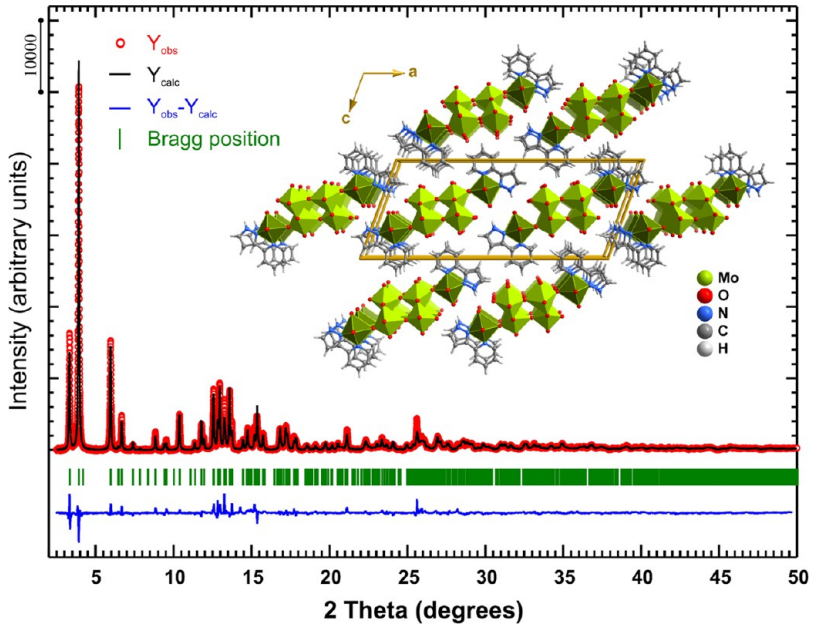

Figure 2. Final Rietveld plot (synchrotron PXRD data) of $[Mo_3O_9(pzpy)]_n$ (**2**). Observed data points are indicated as red circles, and the best fit profile (upper trace) and the difference pattern (lower trace) are drawn as solid black and blue lines, respectively. Green vertical bars indicate the angular positions of the allowed Bragg reflections. Refinement details are given in Table 1. A mixed ball-and-stick and polyhedral crystal packing representation of **2** viewed down the [010] crystallographic direction is provided as an inset.

dx.doi.org/10.1021/ic403033j | Inorg. Chem. 2014, 53, 2652–2665

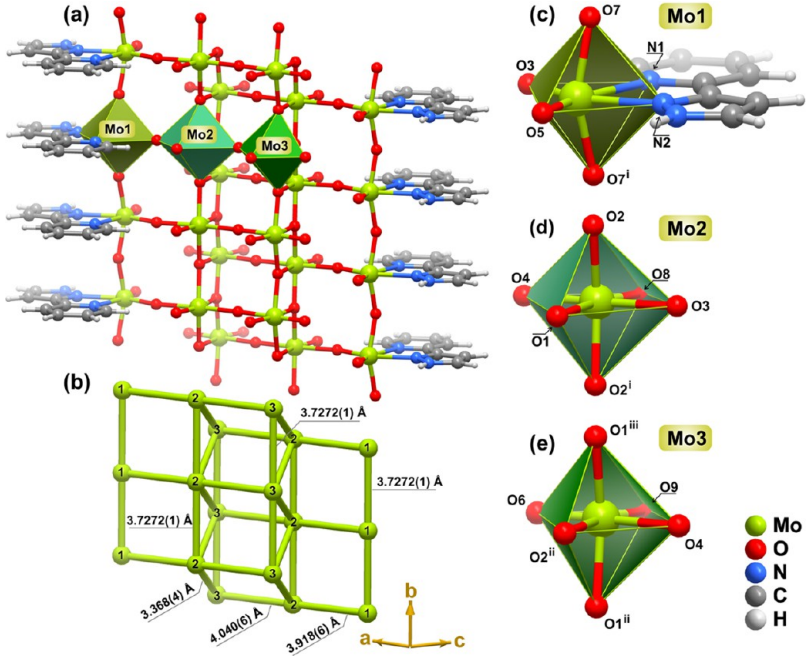

Figure 3. One-dimensional neutral $^{1}_{\infty}[Mo_3O_9(pzpy)]$ hybrid polymer present in the crystal structure of **2** running parallel to the *b* axis, emphasizing (a) the three crystallographically independent Mo^{VI} metal centers and (b) the respective intermetallic distances within the polymer. Schematic representation of the distorted octahedral coordination environments of (c) Mo1, (d) Mo2, and (e) Mo3. Selected bond lengths and angles are listed in Tables 2 and 3. Symmetry transformations used to generate equivalent atoms: (i) *x*, −1 + *y*, *z*; (ii) 1/2 − *x*, −1/2 + y, 1 − *z*; (iii) 1/2 − *x*, 1/2 + y, 1 − *z*.

Table 2. Selected Bond Lengths (Å) for the Three Crystallographically Independent Molybdenum Coordination Environments Present in $[Mo_3O_9(pzpy)]_n$ (2)[a]

Mo1−O3	2.00(2)	Mo1−O7^{i}	1.909(3)
Mo1−O5	1.671(15)	Mo1−N1	2.35(2)
Mo1−O7	1.909(3)	Mo1−N2	2.17(3)
Mo2−O1	2.32(2)	Mo2−O3	2.02(2)
Mo2−O2	1.930(5)	Mo2−O4	2.02(2)
Mo2−O2^{i}	1.930(5)	Mo2−O8	1.691(16)
Mo3−O1^{ii}	1.927(5)	Mo3−O4	2.03(2)
Mo3−O1^{iii}	1.927(5)	Mo3−O6	1.678(17)
Mo3−O2^{ii}	2.325(18)	Mo3−O9	1.702(18)

[a]Symmetry transformations used to generate equivalent atoms: (i) *x*, −1 + *y*, *z*; (ii) 1/2 − *x*, −1/2 + y, 1 − *z*; (iii) 1/2 − *x*, 1/2 + y, 1 − *z*.

Table 3. Selected Bond Angles (deg) for the Three Crystallographically Independent Molybdenum Coordination Environments Present in $[Mo_3O_9(pzpy)]_n$ (2)[a]

O3−Mo1−O5	117.9(8)	O5−Mo1−N2	95.6(9)
O3−Mo1−O7	90.2(6)	O7−Mo1−N1	77.8(4)
O3−Mo1−O7^{i}	90.2(6)	O7^{i} −Mo1−N1	77.8(4)
O3−Mo1−N1	79.7(9)	O7−Mo1−N2	83.0(6)
O3−Mo1−N2	146.5(9)	O7^{i} −Mo1−N2	83.0(6)
O5−Mo1−O7	100.9(5)	O7−Mo1−O7^{i}	155.1(6)
O5−Mo1−O7^{i}	100.9(5)	N1−Mo1−N2	66.8(10)
O5−Mo1−N1	162.4(9)		
O1−Mo2−O2	75.5(5)	O2−Mo2−O4	96.7(5)
O1−Mo2−O2^{i}	75.5(5)	O2^{i} −Mo2−O4	96.7(5)
O1−Mo2−O3	89.8(7)	O2−Mo2−O8	102.6(5)
O1−Mo2−O4	100.0(7)	O2^{i} −Mo2−O8	102.6(5)
O1−Mo2−O8	163.4(8)	O3−Mo2−O4	170.1(8)
O2−Mo2−O2^{i}	149.8(8)	O3−Mo2−O8	73.6(8)
O2−Mo2−O3	85.7(5)	O4−Mo2−O8	96.5(9)
O2^{i} −Mo2−O3	85.7(5)		
O1^{ii} −Mo3−O1^{iii}	150.6(8)	O1^{iii} −Mo3−O9	103.4(6)
O1^{ii} −Mo3−O2^{ii}	75.4(6)	O2^{ii} −Mo3−O4	76.2(7)
O1^{iii} −Mo3−O2^{ii}	75.4(6)	O2^{ii} −Mo3−O6	104.3(7)
O1^{ii} −Mo3−O4	84.9(6)	O2ii −Mo3−O9	162.6(8)
O1^{iii} −Mo3−O4	84.9(6)	O4−Mo3−O6	179.5(8)
O1^{ii} −Mo3−O6	95.3(6)	O4−Mo3−O9	86.4(9)
O1^{iii} −Mo3−O6	95.3(6)	O6−Mo3−O9	93.1(9)
O1^{ii} −Mo3−O9	103.4(6)		

[a]Symmetry transformations used to generate equivalent atoms: (i) *x*, −1 + *y*, *z*; (ii) 1/2 − *x*, −1/2 + *y*, 1 − *z*; (iii) 1/2 − *x*, 1/2 + *y*, 1 − *z*.

$$DI_{angle} = \frac{\sum_{i=1}^{n} |\angle((N,O)-Mo-(N,O))_i - \angle((N,O)-Mo-(N,O))_{ideal}|}{\sum_{i=1}^{n} |\angle((N,O)-Mo-(N,O))_i|} \quad \text{(Equation 2)}$$

where the subscripts *i* and average/ideal correspond to individual and average/ideal bond lengths and angles. For the sake of comparison, the value of DI_{angle} should be, for an octahedron, calculated independently for the cis and trans angles. Even though the initial model by Baur[18] suggested that DI_{angle} should also be calculated with respect to the average values observed for the polyhedra, we believe that only when comparing with the ideal values of an octahedron (i.e., 90 and 180° for the cis and trans angles, respectively) can one derive correct comparative conclusions on the degrees of distortion for each individual Mo^{VI} coordination environment. Having this in mind, the DI_{bond} values for the three crystallographically independent Mo^{VI} metal centers are 0.086, 0.068, and 0.085 for Mo1, Mo2, and Mo3, respectively. The corresponding DI_{angle} values for the cis(trans) angles are 0.120(0.164), 0.101(0.117),

dx.doi.org/10.1021/ic403033j | Inorg. Chem. 2014, 53, 2652−2665

and 0.104(0.096) for Mo1, Mo2, and Mo3, respectively. These results are significantly clearer, indicating that when we compare the polyhedra to the ideal Archimedean solid, Mo1 is significantly more distorted concerning the angle spread, while Mo2 and Mo3 are, as expected, more structurally similar. In addition, we can further conclude that the variation of the distances is approximately identical for all three Mo^{VI} metal centers, with the environment of Mo2 being slightly more regular than the other two.

The three Mo^{VI} polyhedra coalesce along the [010] direction of the unit cell to produce the hybrid organic–inorganic 1D polymer $^1_\infty[Mo_3O_9(pzpy)]$ depicted in Figure 3a. This polymer is truly unique, and it can be divided into two very distinct components. Interconnection between solely the Mo2 and Mo3 polyhedra leads to the formation of a double ladder-type inorganic core reminiscent of the crystal structure of MoO_3 (Figure 4). Indeed, the Mo···Mo intermetallic distances within the inorganic core of $^1_\infty[Mo_3O_9(pzpy)]$ range from 3.368(4) to 4.040(6) Å (Figure 3b), which are very similar to those found in the crystal structure of the inorganic precursor (from ca. 3.43 to 3.96 Å). The small differences are mainly attributed to crystal packing effects in **2** that induce small distortions in the polyhedra so as to promote a more effective packing of the polymers in the solid state. A portion of this inorganic core has already been found by us in a different polymeric material, for which a neutral hybrid $^1_\infty[MoO_3(bipy)]$ polymer cocrystallizes with a ladder-type $^1_\infty[MoO_3(H_2O)]$ inorganic polymer to produce the functional material $\{[(MoO_3)(bipy)]\text{-}[MoO_3(H_2O)]\}_n$.[9] The hybrid and the inorganic polymers are segregated in the crystal structure of the latter, mutually interacting through supramolecular interactions. The inorganic ladder present in $^1_\infty[MoO_3(H_2O)]$ is solely composed of one zigzag chain of Mo^{VI} centers interconnected through μ_3-bridging oxo groups (in contrast to two such ladders in $^1_\infty[Mo_3O_9(pzpy)]$—see Figures 3 and 4), for which the Mo···Mo intermetallic distances along the chain have an average value of ca. 3.44 Å.

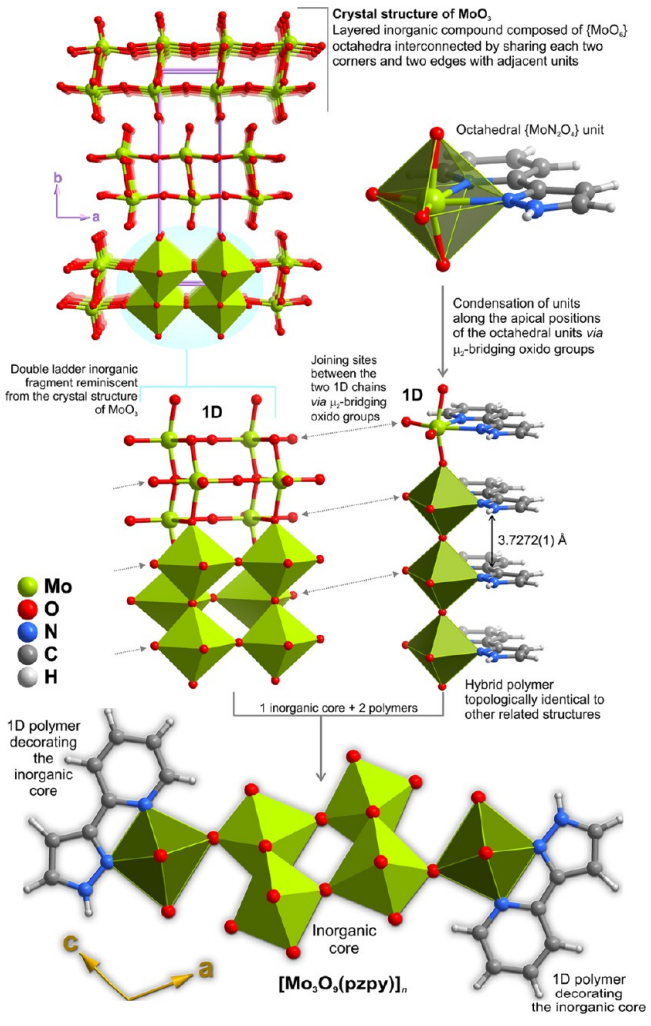

Figure 4. Relationship between the 1D neutral $^1_\infty[Mo_3O_9(pzpy)]$ hybrid polymer present in compound **2** and the topological features reported for related hybrid polymers in the literature and the parent MoO_3 inorganic compound.

Looking only at the structural behavior of the Mo1 polyhedra, the interconnection along the [010] direction via μ_2-bridging oxo groups leads to the formation of a 1D polymer topologically similar to that reported by Zubieta and co-workers in $[MoO_3(bipy)]_n$,[19] and to those described by us in $(DMA)[MoO_3(Hbpydc)]_n{\cdot}H_2O$[11e] and in $\{[MoO_3(bipy)]\text{-}[MoO_3(H_2O)]\}_n$.[9] All these hybrid polymers exhibit a typical **–O–O–O–O–O–** distribution of the oligomeric building units (**O** signifies an octahedral complex with the *N,N*-chelated ligand composing the equatorial plane). Indeed, the Mo···Mo intermetallic distance along this polymer in the compound reported herein [3.7272(1) Å—Figure 3b] compares well with those of the aforementioned structures, which range from ca. 3.61 to 3.76 Å. As found for $[MoO_3(bipy)]_n$ and $\{[MoO_3(bipy)][MoO_3(H_2O)]\}_n$, the *N,N*-chelated moieties in **2** are eclipsed along the grow direction of the polymer (Figure 3).

Connections between the hybrid 1D polymers and the inorganic core in $[Mo_3O_9(pzpy)]_n$ are ensured by a common oxo group, which acts as a μ_2-bridging moiety imposing a Mo···Mo separation of 3.918(1) Å (Figures 3 and 4). In this way, the individual structure composing compound **2** comprises an inorganic core, based on MoO_3, decorated at the periphery by two hybrid polymers. Remarkably, compound **2** finds a structural parallel in the material $\{[MoO_3(bipy)]\text{-}[MoO_3(H_2O)]\}_n$, in which each individual $^1_\infty[MoO_3(H_2O)]$ polymer interacts with two peripheral $^1_\infty[MoO_3(bipy)]_n$ moieties via strong hydrogen bonds.[9]

The crystal structure of **2** is largely dominated by the close packing of individual 1D $^1_\infty[Mo_3O_9(pzpy)]$ polymers, as shown in the inset in Figure 2. The most striking supramolecular contacts present in the structure concern the strong and highly directional N3–H1···O5 hydrogen bonds that, by way of a $R_2^2(10)$ graph set motif,[20] interconnect adjacent 1D polymers, forming supramolecular layers in the *ab* plane of the unit cell (see Table 4 for geometrical details). Figure 5 emphasizes the distribution of these graph sets, which, due to their strong

Table 4. Supramolecular Contacts Present in $[Mo_3O_9(pzpy)]_n$ (2)[a]

D–H···A	*d*(D···A) (Å)	<(DHA) (deg)
N3–H1···O5^{i}	2.88(3)	174
(*intra*) C1–H2···O3	2.84(3)	121
(*intra*) C1–H2···O8	3.15(3)	179

[a]Symmetry transformation used to generate equivalent atoms: (i) 1 − *x*, *y*, 1 − *z*.

dx.doi.org/10.1021/ic403033j | Inorg. Chem. 2014, 53, 2652–2665

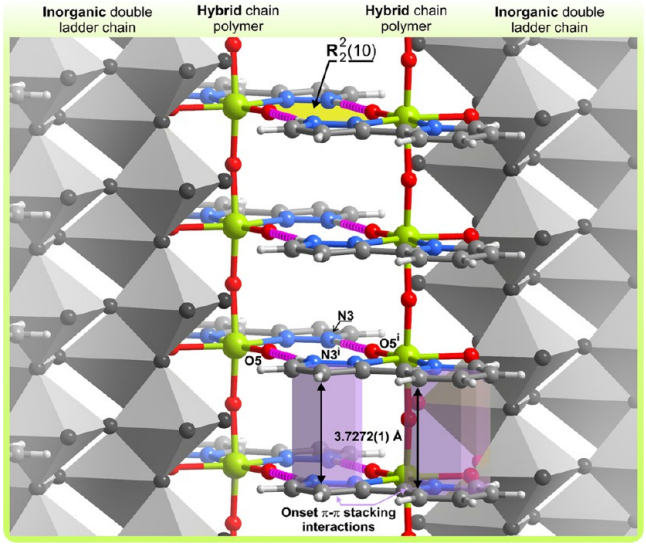

Figure 5. Detailed view of the strong and highly directional N−H···O hydrogen bonding interactions (dashed purple lines) interconnecting adjacent neutral 1D $^1_\infty[Mo_3O_9(pzpy)]$ hybrid polymers, describing $R_2^2(10)$ graph set motifs[20] along the direction of the polymers. Onset $\pi-\pi$ stacking interactions involving the pyridine and pyrazole rings of the organic ligand are represented in violet (intercentroid distances of 3.7272(1) Å). Table 4 gives geometrical details on the represented interactions. Symmetry transformation used to generate equivalent atoms: (i) $1-x, y, 1-z$.

cooperative effect along the [010] direction, increase the structural robustness of compound **2**. There are also a handful of weaker supramolecular interactions, particularly onset $\pi-\pi$ stacking interactions involving the pyridine and pyrazole rings of the organic ligand (Figure 5), and some weak intrapolymer C−H···O hydrogen bonds (see Table 4 for geometrical details).

A search in the literature concerning related polymeric structures (i.e., Mo^{VI} inorganic cores coordinated to *N,N*-chelated ligands) showed unequivocally that **2** was the one with the highest metal content (concerning the metal/ligand ratio) found to date: $(DMA)[MoO_3(Hbpydc)]_n \cdot H_2O$ with 1:1,[11e] $\{[MoO_3(bipy)][MoO_3(H_2O)]\}_n$ with 2:1,[9] $[MoO_3(bipy)]_n$ with 1:1,[19] $[Mo_2O_6(bipy)]_n$ with 2:1,[19] $[Mo_3O_9(bipy)_2]_n$ with 3:2,[19] $[Mo_3O_8(bipy)_2]_n$ with 3:2,[21] $[Mo_4O_{12}(bipy)_3]_n$ with 4:3,[22] and $[Mo_3O_9(phen)_2]_n$ with 3:2 (where phen = 1,10-phenanthroline).[23−25] These prior results clearly show that the Mo content is never above 2 (in relation to the organic ligand), with this circumstance only occurring in exceptional cases for materials containing a large fraction of inorganic components (*please note*: we have excluded from this search compounds having isolated polyoxometalates[26,27] as templates): while in $\{[MoO_3(bipy)][MoO_3(H_2O)]\}_n$ the material is composed of a hybrid 1D structure cocrystallizing with a purely inorganic polymer,[9] in $[Mo_2O_6(bipy)]_n$ reported by Zubieta and co-workers[19] the polymer is instead formed by alternating octahedral complexes (**O**, having the *N,N*-chelated ligand composing the equatorial plane) and tetrahedral (**T**) MoO_4^{2-} inorganic units in a typical **−O−T−O−T−O−** fashion.

Single-Crystal X-ray Structure of 5. Compound $[MoO(O_2)_2(pzpy)]$ (**5**) crystallizes in the centrosymmetric orthorhombic space group *Pbca* (Table 5) with the asymmetric unit being composed of a whole molecular unit, as depicted in Figure 6. The single Mo^{VI} metal center is coordinated to one *N,N*-chelated pzpy organic moiety, two peroxo groups, and one terminal oxo group. A search in the literature and in the Cambridge Structural Database (Version 5.34, November 2012 with three updates[28]) reveals the existence of a handful of related structures (i.e., sharing the same coordination environment) with various types of *N,N*-chelating organic ligands bound to the metal center.[12b,c,29] The coordination environment of Mo^{VI} in all these structures is identical to that found in compound **5**: (i) overall coordination number of 7 (see Table 6 for selected bond lengths and angles concerning the coordination polyhedron); (ii) two peroxo groups are cis-positioned with respect to the oxo one.

The oxo group in **5** exerts its typical trans effect, pulling the Mo^{VI} from the average equatorial plane by ca. 0.37 Å. This displacement value falls well within the range observed in the aforementioned related structures: from ca. 0.30 to 0.40 Å with a median value of 0.36 Å.[12b,c,29] This trans effect is concomitantly accompanied by the presence of a much longer Mo−N bond length [Mo1−N3 = 2.358(3) Å—see Table 5]; this value in $[MoO(O_2)_2(pzpy)]$ is, nevertheless, well within the expected range (from ca. 2.29 to 2.43 Å with median of ca. 2.35 Å). As shown in Figure 6, the equatorial plane of the coordination polyhedron is composed of the two peroxo groups and the nitrogen atom from the pyrazole ring. In a simplified approach, taking the centers of gravity of the latter moieties as the coordination sites (i.e., $C_{gO1,O2}$ and $C_{gO3,O4}$), the overall coordination environment can be envisaged as a highly distorted trigonal bipyramid: the cis equatorial and apical polyhedral angles are found in the ca. 107.8−130.2° and 70.1−105.3° ranges, respectively, and the Mo1−(N,O,C_g) distances

Table 5. Crystal and Structure Refinement Data for $[MoO(O_2)_2(pzpy)]$ (5)

formula	$C_8H_7MoN_3O_5$
formula weight	321.11
crystal system	orthorhombic
space group	*Pbca*
a (Å)	15.1933(14)
b (Å)	8.4300(8)
c (Å)	15.4515(13)
volume (Å)^3	1979.0(3)
Z	8
D_c (g cm^{-3})	2.155
μ(Mo Kα) (mm^{-1})	1.341
crystal size (mm)	0.06 × 0.03 × 0.02
crystal type	yellow blocks
θ range	3.61 to 29.13
index ranges	$-15 \le h \le 20$
	$11 \le k \le 11$
	$-21 \le l \le 21$
reflections collected	31707
independent reflections	2660 [R_{int} = 0.0742]
completeness to θ = 29.13°	99.8%
final *R* indices [$I > 2\sigma(I)$]^{a,b}	*R*1 = 0.0460
	*wR*2 = 0.0697
final *R* indices (all data)^{a,b}	*R*1 = 0.0700
	*wR*2 = 0.0751
weighting scheme^c	*m* = 0.0220
	n = 5.9988
largest diff. peak and hole	0.973 and −0.767 e Å^{-3}

$^a R1 = \sum||F_o| - |F_c||/\sum|F_o|$. $^b wR2 = (\sum[w(F_o^2 - F_c^2)^2]/\sum[w(F_o^2)^2])^{1/2}$ $^c w = 1/[\sigma^2(F_o^2) + (mP)^2 + nP]$ where $P = (F_o^2 + 2F_c^2)/3$

dx.doi.org/10.1021/ic403033j | *Inorg. Chem.* 2014, 53, 2652−2665

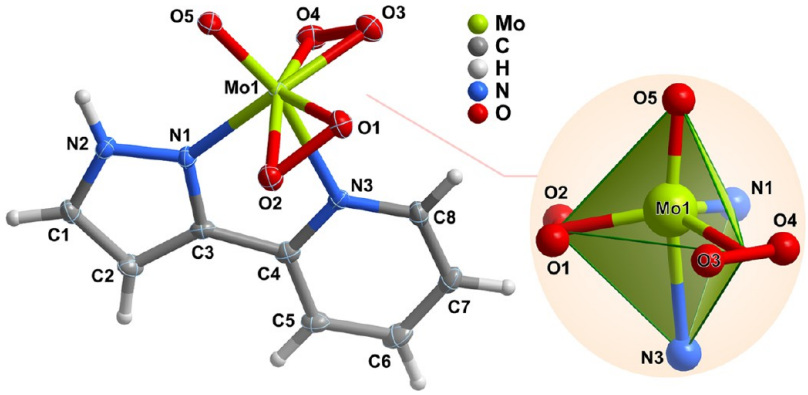

Figure 6. Schematic representation of the crystallographically independent molecular unit composing the asymmetric unit of $[MoO(O_2)_2(pzpy)]$ (**5**). Non-hydrogen atoms are represented as thermal ellipsoids drawn at the 50% probability level. Hydrogen atoms are represented as small spheres with arbitrary radii. The inset emphasizes the distorted trigonal bipyramidal coordination environment of Mo1 when each peroxide ligand is considered as a single coordination site. Table 6 lists selected bond lengths and angles.

Table 6. Bond Distances (Å) and Angles (deg) for the Crystallographically Independent Mo^{VI} Metal Center Present in $[MoO(O_2)_2(pzpy)]$ (5)

Mo1−O1	1.902(3)	Mo1−O5	1.689(2)
Mo1−O2	1.945(3)	Mo1−N1	2.157(3)
Mo1−O3	1.916(3)	Mo1−N3	2.358(3)
Mo1−O4	1.974(3)		
Mo1−$C_{gO1,O2}$	1.779(3)	Mo1−$C_{gO3,O4}$	1.805(3)
O1−Mo1−O2	44.67(11)	O3−Mo1−N3	85.81(10)
O1−Mo1−O3	88.40(11)	O4−Mo1−N1	89.40(11)
O1−Mo1−O4	130.25(11)	O4−Mo1−N3	78.52(10)
O1−Mo1−N1	129.65(11)	O5−Mo1−O1	106.31(11)
O1−Mo1−N3	86.99(10)	O5−Mo1−O2	102.07(11)
O2−Mo1−O4	157.32(10)	O5−Mo1−O3	105.65(11)
O2−Mo1−N1	86.26(11)	O5−Mo1−O4	100.34(11)
O2−Mo1−N3	79.07(9)	O5−Mo1−N1	92.34(10)
O3−Mo1−O2	130.81(11)	O5−Mo1−N3	162.39(11)
O3−Mo1−O4	43.68(10)	N1−Mo1−N3	70.13(10)
O3−Mo1−N1	131.46(11)		

are spread in the wide 1.689(2)−2.358(3) Å range (Table 6 and Figure 6).

Even though the complex $[MoO(O_2)_2(pzpy)]$ (**5**) is rich in atoms capable of acting as acceptors in strong hydrogen bonds (due to the presence of various terminal oxygen atoms), there are not many donor groups in the crystal structure that can facilitate these supramolecular interactions. It is thus not surprising that the crystal packing of **5** is mostly mediated by the maximization of the sole N2−H1···O4 hydrogen bond present in the crystal structure (Figure S7 in the Supporting Information). This interaction, very strong and highly directional (see Supporting Information, Table S4 for geometrical parameters), occurs between neighboring individual complexes leading to the formation of a $C_1^1(5)$ graph set motif parallel to the *b* axis of the unit cell.[20] Each complex is involved in two such motifs in the *ab* plane, which creates a 2D supramolecular layer (Supporting Information, Figure S8). Besides this strong interaction, a handful of C−H groups from the organic ligand are engaged in weak C−H···O interactions (not shown; see Supporting Information, Table S4 for geometrical details).

Spectroscopic Characterization. Compound **2** was further characterized by $^{13}C\{^1H\}$ CP MAS NMR, FT-IR, and FT-Raman spectroscopies. The $^{13}C\{^1H\}$ CP MAS NMR spectrum displays several sharp signals between 100 and 150 ppm that can be readily assigned to the eight carbon atoms of the pyrazolylpyridine ligand (Figure S9 in the Supporting Information).

Table 7 lists the most characteristic and representative metal−ligand vibrations calculated and experimentally observed for compounds **1**, **4**, and **5**. Overall, there is a good qualitative agreement between experimental and calculated values despite the simplification of the calculated model, namely, only the isolated molecules are considered. Because of the large size of the system, no computational investigation was performed for **2**, and tentative band assignments are based on the information provided by the comparison with the other molybdenum

Table 7. Selected Raman and IR bands (cm^{-1}) for 1, 4, and 5, and Calculated (B3LYP) Values

complex	calcd[a]	IR[b]	Raman	assignment
1	932	940s	937vs	$\nu(Mo{=}O)_{sym}$
	918	906vs	909s	$\nu(Mo{=}O)_{asym}$
	337	395w	397m	$\gamma(MoO_2)$
	308	345m		$\nu(Mo{-}Cl)_{asym}$
	276		222m	$\nu(Mo{-}Cl)_{sym}$
	151		171w	$\nu(Mo{-}N)_{sym}$
	137			$\nu(Mo{-}N)_{asym}$
4	857		900s	$\nu(Mo{=}O)_{sym}$
	850		908sh	$\nu(Mo{=}O)_{asym}$
	802	818/849s	812/848s	$\nu(Mo{-}O{-}Mo)_{asym}$
	348	436m		$\delta(Mo{-}O{-}Mo)$
	331	402s	403m	$\nu(Mo{-}O{-}Mo)_{sym}$
	322	343m	342m	$\gamma(MoO_2)$
5	929	950vs[c]	955w[c]	$\nu(Mo{=}O)$
	876	875sh	873s	$\nu(O{-}O)_{sym}$
	875	864s	862sh	$\nu(O{-}O)_{asym}$
	583	584s	585m	$\nu(Mo{-}O)_{peroxo}$
	543	539m	538m	$\nu(Mo{-}O)_{peroxo}$
	494	512s	511m	$\nu(Mo{-}O)_{peroxo}$
	463	492m	492w	$\nu(Mo{-}O)_{peroxo}$
	298	393m	393m	$\gamma(O{=}Mo(O_2)_2)$
	160		187w	$\nu(Mo{-}N)_{sym}$
	103			$\nu(Mo{-}N)_{asym}$

[a]Scaled values (scale factor = 0.961). [b]Abbreviations: sh = shoulder, vs = very strong, vw = very weak, m = medium, w = weak. [c]Overlap with strong pyrazole ring deformation mode of the pzpy ligand.

dx.doi.org/10.1021/ic403033j | Inorg. Chem. 2014, 53, 2652−2665

systems described herein as well as on the literature data found for related molybdenum[30] and tungsten[31] compounds.

The bands arising from Mo═O vibrations are intense and characteristic in the IR and Raman spectra of *cis*-dioxo complexes, being expected two Mo═O stretching modes (ν(Mo═O)) and a deformation mode $\gamma(MoO_2)$.[32] For compounds **1** and **2**, the pairs of intense IR bands at 906/940 cm^{-1} and (930/935/941)/967 cm^{-1} are assigned to the asymmetric and symmetric stretching vibrations of the *cis*-$[MoO_2]^{2+}$ core (Figure 7), while for complex **4** only a strong

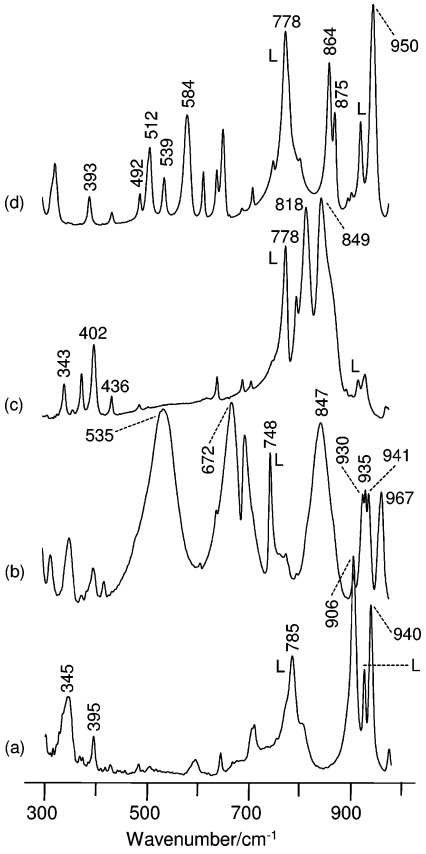

Figure 7. FT-IR spectra in the 300−1000 cm^{-1} region for (a) complex **1**, (b) compound **2**, (c) tetranuclear complex **4**, and (d) oxodiperoxo complex **5**.

Raman band at 900 cm^{-1} and a shoulder at 908 cm^{-1} are observed (not shown). The bands observed at ca. 921 and 929 cm^{-1} and identified in Figure 7 as L are assigned to vibrations with dominant contribution from the pzpy ligand.

The expected out-of-plane deformation mode $\gamma(MoO_2)$, a useful characteristic to recognize the *cis*-$[MoO_2]^{2+}$ core, occurs at 397 cm^{-1} in the Raman spectrum of complex **1** and shifts to lower wavenumbers (343 and 342 cm^{-1}) for the hybrid material **2** and the tetranuclear complex **4**, respectively (Figure 8). For complex **5**, containing bidentate chelating peroxo groups, this $\gamma(MoO_2)$ band is not expected in the vibrational spectra. However, a Raman band at a similar wavenumber of 393 cm^{-1} is observed and can be tentatively assigned to the out-of-plane deformation mode (γ) of the O═Mo$(O_2)_2$ group. A comparison with the vibrational spectra of [MoO$(O_2)_2$Cl(pzpyH)][6c] supports this assignment (this band is apparently absent from the spectra) as in this structure a heavy chlorine

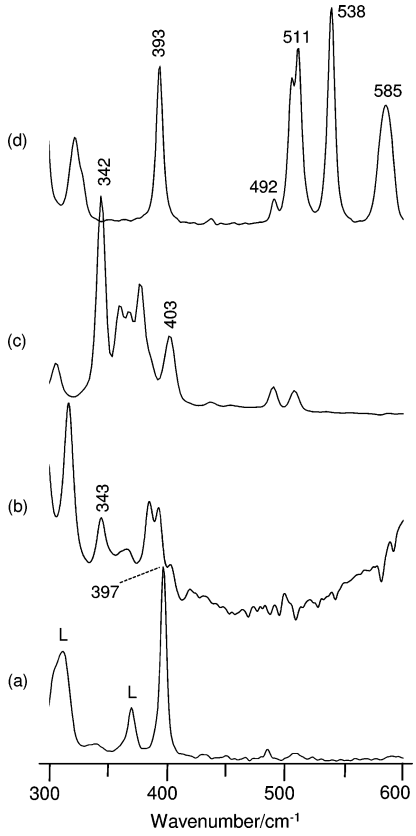

Figure 8. FT-Raman spectra in the 300−600 cm^{-1} region for (a) complex **1**, (b) compound **2**, (c) tetranuclear complex **4**, and (d) oxodiperoxo complex **5**.

atom was attached to the O═Mo$(O_2)_2$ group, therefore preventing a higher displacement of this mode.

The presence of molybdenum systems with higher complexity in compounds **2** and **4** is indicated by the IR bands related to the bridging Mo−O−Mo unit, which are not present in the spectrum of **1** (Figure 7). On the basis of the DFT calculations performed for **4**, the band at 402 cm^{-1} is assigned as the symmetric stretching mode, ν(Mo−O−Mo)$_{sym}$, while the band at 436 cm^{-1} is assigned to the out-of-plane deformation δ(Mo−O−Mo). The pair of strong bands assigned to the Mo−O asymmetric stretching vibration of the Mo−O−Mo bridge appears at 818/849 cm^{-1}, in agreement with previous studies.[29d,33] For compound **2**, while the ν(Mo−O−Mo)$_{asym}$ mode appears as a broad IR band at 847 cm^{-1} (similar to complex **4**), the broad IR bands at 672 and 535 cm^{-1} can be attributed to δ(Mo−O−Mo) and ν(Mo−O−Mo)$_{sym}$ modes, respectively, somewhat higher than those observed for **4**. These shifts to higher wavenumbers can be explained by the large decrease in the degree of linearity of the oxide bridges between the two Mo^{VI} centers on going from compound **4** (Mo−O−Mo = 175.4°) to **2** (Mo−O−Mo = 155.1°). Additionally, the C−H out-of-plane bending mode of the pzpy ligand observed at 785 cm^{-1} for complex **1** and at 778 cm^{-1} for complexes **4** and **5** shifts to lower wavenumber, at 748 cm^{-1}, for **2**.

The vibrational Mo═O and O−O stretching modes for complex **5** are clearly distinguished in the spectrum as sharp and very strong bands. The IR spectrum (Figure 7d) shows the ν(Mo═O) band at 950 cm^{-1}, while two bands at 875 and 864 cm^{-1} are found for the asymmetric and symmetric peroxo stretching ν(O−O) modes, respectively. Additionally, four

dx.doi.org/10.1021/ic403033j | Inorg. Chem. 2014, 53, 2652−2665

bands assigned to the metal−peroxo stretching modes ν(Mo−O)$_{peroxo}$ appear in both the IR (584, 539, 512, 492 cm^{-1}, Figure 7d) and Raman (585, 538, 511, 492 cm^{-1}, Figure 8d) spectra. The observed ν(Mo═O) and ν(O−O) wavenumbers are similar to the values reported for related compounds.[29b−d] The bands identified in Figure 8 as L are assigned to pzpy ligand vibrations.

The detailed analysis of the vibrational spectra of compounds **1**, **2**, **4**, and **5** in the 1550−1650 cm^{-1} region (data not shown) demonstrates structural changes in the pzpy ligand upon complexation. In this region, the bands arising from the ligand N−C−C−N fragment, from the C−C pyridine vibrations, and from the C−N ring stretching vibrations, reflect the general trend, observed for other complexes, of shifting to higher wavenumbers upon coordination to the Mo^{VI} center, in agreement with previous studies.[6c,12d] The bands of pzpy at 1565 cm^{-1} (pzpy C−C inter-ring stretching mode), 1590 cm^{-1} (py C−N stretching mode), and 1597 cm^{-1} (py C−C stretching mode) are shifted to 1570/1613, 1570/1607, 1567/1607, and 1570/1610 cm^{-1} for compounds **1**, **2**, **4**, and **5**, respectively.

Catalysis. The catalytic performance of **2** was investigated for the model epoxidation reaction of *cis*-cyclooctene (Cy) using *tert*-butylhydroperoxide (TBHP, in decane) as oxidant, at 55 or 75 °C, without cosolvent (denoted nosolv) or using an organic cosolvent (1,2-dichloroethane (DCE) or *α,α,α*-trifluorotoluene (TFT); Figure 9 and Table 8). For all reaction conditions using **2** as catalyst, 1,2-epoxycyclooctane (CyO) was the only reaction product (100% selectivity). In contrast, when no catalyst was added, 1,2-cyclooctanediol was formed in 2−10% yields when reacted at 75 °C for 24 h. Hence, the molybdenum species plays an important role in the selective epoxidation of the olefin.

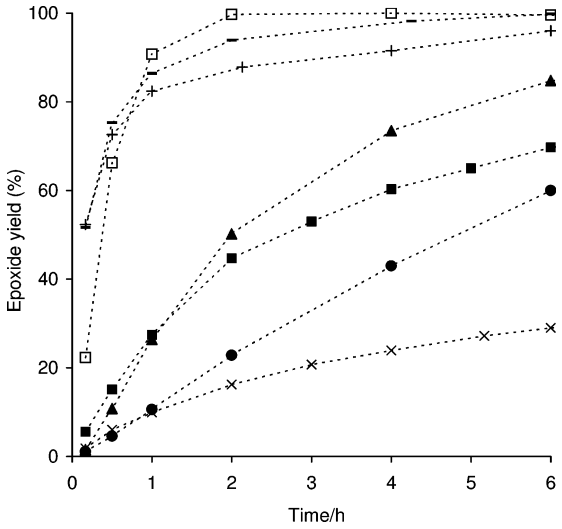

Figure 9. *cis*-Cyclooctene epoxidation with TBHP (using an initial molar ratio of Mo/olefin/TBHP = 1:100:152 for **2** and 0.3:100:152 for **5**) for systems **2**/55 °C/nosolv (×), **2**/75 °C/nosolv (■), **2**/75 °C/TFT (●), **2**/75 °C/DCE (▲), and **5**/75 °C/DCE (□). Dissolv_Test profiles are also given for the **2**/75 °C/TFT (+) and **2**/75 °C/DCE (−) systems. 1,2-Epoxycyclooctane was the only reaction product. The dashed lines are visual guides.

The reaction of Cy with TBHP in the presence of **2** at 55 °C gave 29 and 51% CyO yields at 6 and 24 h reaction times, respectively. These results are inferior to those reported previously for mononuclear or tetranuclear molybdenum complexes bearing the same ligand and tested as (pre)catalysts for the same reaction under similar conditions (Table 9).[6c,12e] The different catalytic performances may be partly due to polymeric **2** having a lower amount of effective active species in comparison to the mono and tetranuclear complexes and/or to differences in catalyst stability. A comparison of the catalytic results for **2** with those reported in the literature for polymeric molybdenum-containing compounds bearing organic ligands different from pzpy, tested as (pre)catalysts in the same reaction under similar conditions, shows that the catalytic activity of **2** (based on CyO yield at 24 h, 55 °C, nosolv) is comparable to that of [Mo_2O_6(HpypzA)] (57%),[10] inferior to that of [MoO_3(bipy)]$_n$ (78%)[9] and [Mo_8O_{24}(pypzEA)$_4$] (100%),[12e] and superior to that of {[MoO_3(bipy)]-[MoO_3(H_2O)]}$_n$ (34%).[9]

Increasing the reaction temperature from 55 to 75 °C led to faster reaction of Cy: 70% CyO yield at 6 h and quantitative CyO yield at 24 h. It has been reported for hybrid organic−inorganic molybdenum-containing polymers that the use of halogenated and noncoordinating cosolvents such as DCE and TFT may have a beneficial effect on the catalytic reaction rate of Cy with TBHP.[9,10] For **2**, at least 98% conversion was reached at 24 h, using these cosolvents (or nosolv) at 75 °C, and CyO was always the only product (Table 8). Differences in reaction rates were observed in the initial stages: conversion at 6 h followed the order DCE > nosolv > TFT (Figure 9). The catalytic performance of **2** using DCE at 75 °C is comparable to that reported for [Mo_8O_{24}(di-*t*Bu-bipy)$_4$], which led to 100% CyO yield at 24 h.[30]

The CatFilt_Test (details given in the Experimental Section) was carried out for the nosolv, TFT, and DCE solvent systems at 75 °C. Without adding a catalyst, the conversions at 6(24) h were 6(13)%, 3(5)% and 2(4)%, respectively. The ratio of Δ*F*iltCat/Δnone was always greater than unity, suggesting that a homogeneous catalytic contribution existed (Table 8). However, for each solvent system the value of Δ*F*iltCat was much smaller than the increment in conversion observed in the presence of **2** (without filtration) for the same time interval. These results suggest that the filtration led to the removal of insoluble active species, or the dissolution of metal species was slow and interrupted by the filtration step. The Dissolv_Test (details given in the Experimental Section) experiment was carried out for the solvent systems DCE and TFT at 75 °C (filtration was carried out at 24 h, whereas for the CatFilt_Test it was carried out at 2 h reaction). The catalytic results were roughly similar for the two solvents, and the reaction rates were much higher than those for the corresponding typical catalytic tests (Figure 9). These results suggest that **2** acts as a source of soluble active species (ruling out the existence of a heterogeneous catalytic species), and the type of soluble active species is possibly similar for the two cosolvents. The greater value of Δ*F*iltCat/Δnone for DCE in comparison to TFT is possibly due to the higher solubility of the active species in the former solvent.

In an attempt to isolate and identify the soluble species, a large-scale (30-fold increase) experiment was carried out for **2**/TBHP/DCE (without olefin; please see the Experimental Section for details). Addition of pentane and diethyl ether to the liquid phase resulted in the precipitation of a pale-yellow solid, which was identified as the oxodiperoxo complex [$MoO(O_2)_2$(pzpy)] (**5**) by elemental analysis, single-crystal X-ray diffraction, PXRD, FT-IR, and NMR spectroscopy. Thiel

dx.doi.org/10.1021/ic403033j | *Inorg. Chem.* 2014, 53, 2652−2665

Table 8. Epoxidation of *cis*-Cyclooctene with TBHP in the Presence of 2, and the Catalytic Results for the Dissolv_Test[a]

cosolvent	reaction temperature (°C)	epoxide yield (%) at 6/24 h reaction[b]	ΔFiltCat/Δnone[c]
none	55	29/51	
none	75	70/98	2
TFT	75	60/100	2
DCE	75	85/100	6
TFT (Dissolv_Test)[c]	75	96/99	
DCE (Dissolv_Test)[c]	75	100/100	

[a]Reaction conditions: initial molar ratios of Mo/Cy/TBHP ≅ 1:100:152, initial concentration of Cy = 1 M. [b]The epoxide was always the only reaction product. [c]Details for ΔFiltCat/Δnone and Dissolv_Test are given in the Experimental Section.

Table 9. Epoxidation of *cis*-Cyclooctene with TBHP in the Presence of Molybdenum Compounds Possessing the Ligand L = pzpy[a]

compound	epoxide yield (%) at 6/24 h reaction[b]	metal species[c]	ref
$[Mo_3O_9(pzpy)]_n$ (**2**)	29/51	LP = $[MoO(O_2)_2L]$ (**5**)	this Work
$[MoO_2Cl_2L]$	67/90	SP = unknown polymer or molybdenum oxide cluster	6c
$[MoO_2(OSiPh_3)_2L]$	65/90	SP = $[Mo_4O_{12}L_4]$ (**4**)	6c
$[Mo(CO)_4L]$	51/78	SP = $[Mo_4O_{12}L_4]$ (**4**)	12e
$[Mo_4O_{12}L_4]$ (**4**)	55/92	SP = $[Mo_4O_{12}L_4]$ (**4**)	12e

[a]Reaction conditions: molar ratios of Mo/Cy/TBHP ≅ 1:100:152, without cosolvent, 55 °C. [b]The epoxide was always the only reaction product. [c]Metal species identified or characterized after a 24 h catalytic batch run. SP (solid phase) denotes the recovered solid, and LP (liquid phase) denotes the solid isolated from solution by precipitation with an organic solvent.

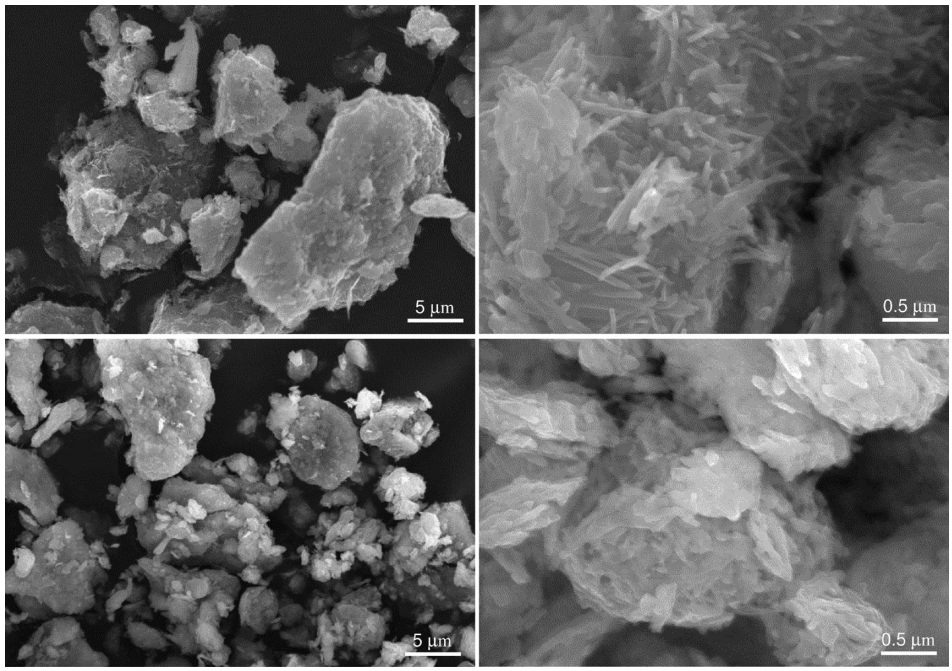

Figure 10. SEM images. (top) Compound **2**. (bottom) The solid recovered after the catalytic run **2**/75 °C/TFT.

et al. reported the catalytic performance of **5** for the reaction of Cy with TBHP (at 30, 50, or 65 °C; chloroform or toluene as cosolvent; TBHP in chloroform).[12a] A catalytic test was carried out for **5** (TBHP/DCE/75 °C) using an equivalent molar amount of complex as that used for **2** under typical reaction conditions; this amount of **5** used corresponds to that calculated assuming that the moieties of **2** which possess a pzpy ligand are completely transformed into species of the type **5**, in a 1:1 stoichiometric ratio. The reaction was complete within 2 h, indicating that **5** is a very active catalyst (Figure 9). These results are somewhat consistent with the relatively fast reaction of Cy for the Dissolv_Test experiments. Hence, it seems that **2** is poorly soluble in the reaction media, and it is gradually converted into the soluble complex **5**, which is at least partly responsible for the homogeneous catalytic reaction of Cy. The conversion of **2** to **5** necessarily forms molybdenum coproducts (the two compounds possess different Mo/ligand ratios), and structural modifications of **2** are expected. However, the PXRD patterns and attenuated total reflection FT-IR spectra of the solids recovered after 24 h of reaction of Cy (denoted **2**-nosolv-75, **2**-DCE-75, and **2**-TFT-75 for a reaction temperature of 75 °C, and **2**-nosolv-55 for the nosolv system at 55 °C) were very similar to that for **2** (Figures S10 and S11 in the Supporting Information). If the coproducts were insoluble, then they were amorphous and/or formed in insufficient amounts to be detected. On the other hand, it is

dx.doi.org/10.1021/ic403033j | Inorg. Chem. 2014, 53, 2652−2665

possible that the coproducts are soluble and difficult to isolate. Some morphological changes were apparent in the scanning electron microscopy (SEM) images of the recovered solids, showing reduction in particle sizes of **2** (exemplified in Figure 10 for the TFT system at 75 °C). These changes may be related to the fragmentation of **2** to **5**.

CONCLUSIONS

The hydrolysis and condensation of complexes of the type $[MoO_2Cl_2L]$ has proven to be a fascinating route to molybdenum oxide/organic assemblies. To date the following compounds have been prepared and structurally characterized: $\{[MoO_3(bipy)][MoO_3(H_2O)]\}_n$,[9] $[Mo_8O_{22}(OH)_4(di\text{-}tBu\text{-}bipy)_4]$,[8] $[Mo_2O_6(HpypzA)]$,[10] and in this Work $[Mo_3O_9(pzpy)]_n$. In a manner analogous to that commonly encountered in sol−gel chemistry,[34] hydrolysis of the Mo−Cl bonds in the molecular precursors likely gives reactive Mo−OH species that condense through oxolation and/or olation reactions to give metal-oxo clusters, oligomers, and polymers assembled via M−O−M and/or M−OH−M bridges. In general the reactions are highly reproducible and give good to very good yields of the hybrid materials. The distinct nature of the solid-state structures for these four materials clearly demonstrates the structure-directing influence of the organic ligands. Of all the molybdenum oxide/organic hybrid materials reported so far, $[Mo_3O_9(pzpy)]_n$ (**2**) is the one with the highest metal/ligand ratio. It finds a structural parallel in the material $\{[MoO_3(bipy)][MoO_3(H_2O)]\}_n$, in which each individual $^1_\infty[MoO_3(H_2O)]$ polymer interacts with two peripheral $^1_\infty[MoO_3(bipy)]_n$ moieties via strong hydrogen bonds. In **2** the MoO_3-based inorganic core is, however, linked covalently at the periphery to two hybrid polymers consisting of corner-sharing distorted $\{MoO_4N_2\}$ octahedra.

When material **2** is used in catalytic olefin epoxidation, it acts as a source of soluble active species, which include but may not be limited to the oxodiperoxo complex $[MoO(O_2)_2(pzpy)]$. We may assume that these species originate from the corner-sharing $\{MoO_4N_2\}$ units that make up the 1D hybrid polymer component in **2**.

Work is ongoing in our laboratory to further explore the aqueous chemistry of $[MoO_2Cl_2L]$ complexes, with the intention of expanding the structural diversity of molybdenum oxide/organic hybrid materials.

ASSOCIATED CONTENT

Supporting Information

PXRD patterns (Figures S1, S2, and S10), crystallographic information files (CIF) for compounds **2**, **3**, and **5**, detailed crystallographic description of all crystal structures, including technical structure solution and refinement details (Tables S1−S3, Figures S3−S6), additional crystallographic table (Table S4) and representations (Figures S7 and S8) of **5**, $^{13}C\{^1H\}$ CP MAS NMR spectrum of **2** (Figure S9), and ATR FT-IR spectra (Figure S11). This material is available free of charge via the Internet at http://pubs.acs.org. Crystallographic data for compounds **2**, **3**, and **5** reported in this Article have been deposited at the Cambridge Crystallographic Data Centre as CCDC 969882, 969692, and 970348, respectively. These data can be obtained free of charge from the Cambridge Crystallographic Data Centre via www.ccdc.cam.ac.uk/conts/retrieving.html.

AUTHOR INFORMATION

Corresponding Authors

*E-mail: igoncalves@ua.pt (I.S.G.).
*E-mail: filipe.paz@ua.pt (F.A.A.P.).

Notes

The authors declare no competing financial interest.

ACKNOWLEDGMENTS

The Portuguese group is grateful to the Fundação para a Ciência e a Tecnologia (FCT), QREN, Fundo Europeu de Desenvolvimento Regional (FEDER), COMPETE, and the European Union for funding (R&D Projects No. PTDC/EQU-EQU/121677/2010 and No. PDTC/QUI-QUI/098098/2008 (FCOMP-01-0124-FEDER-010785)). The Swiss group thanks the Swiss National Science Foundation for funding. The Associate Laboratory CICECO (PEst-C/CTM/LA0011/2013) is acknowledged for continued support and funding. The FCT and the European Union are acknowledged for a postdoctoral Grant to P.N. (SFRH/BPD/73540/2010) cofunded by MCTES and the European Social Fund through the program POPH of QREN, and for a Ph.D. Grant to T.R.A. (SFRH/BD/64224/2009). We thank the Diamond Light Source (DLS) for access to beamline I11 (EE8234) that contributed to the results presented here, and also Dr. Stephen Thomson for help during the experiment. The research leading to these results has received funding from the European Community's Seventh Framework Programme (FP7/2007-2013) under Grant Agreement No. 226716. F.A.A.P. also wishes to thank Chevron (Richmond, CA, USA) for funding a research visit to ETH Zürich.

REFERENCES

(1) (a) Jeyakumar, K.; Chand, D. K. *J. Chem. Sci.* **2009**, *121*, 111. (b) Sanz, R.; Pedrosa, M. R. *Curr. Org. Synth.* **2009**, *6*, 239. (c) Noronha, R. G.; de Fernandes, A. C. *Curr. Org. Synth.* **2012**, *16*, 33.

(2) (a) Nunes, C. D.; Valente, A. A.; Pillinger, M.; Rocha, J.; Gonçalves, I. S. *Chem.—Eur. J.* **2003**, *9*, 4380. (b) Arnáiz, F. J.; Aguado, R.; Pedrosa, M. R.; Cian, A. D. *Inorg. Chim. Acta* **2003**, *347*, 33. (c) Gago, S.; Neves, P.; Monteiro, B.; Pessêgo, M.; Lopes, A. D.; Valente, A. A.; Paz, F. A. A.; Pillinger, M.; Moreira, J.; Silva, C. M.; Gonçalves, I. S. *Eur. J. Inorg. Chem.* **2009**, 4528. (d) Kühn, F. E.; Herdtweck, E.; Haider, J. J.; Herrmann, W. A.; Gonçalves, I. S.; Lopes, A. D.; Romão, C. C. *J. Organomet. Chem.* **1999**, *583*, 3.

(3) Kühn, F. E.; Lopes, A. D.; Santos, A. M.; Herdtweck, E.; Haider, J. J.; Romão, C. C.; Santos, A. G. *J. Mol. Catal. A: Chem.* **2000**, *151*, 147. (b) Kühn, F. E.; Groarke, M.; Bencze, É.; Herdtweck, E.; Prazeres, A.; Santos, A. M.; Calhorda, M. J.; Romão, C. C.; Gonçalves, I. S.; Lopes, A. D.; Pillinger, M. *Chem.—Eur. J.* **2002**, *8*, 2370. (c) Günyar, A.; Betz, D.; Drees, M.; Herdtweck, E.; Kühn, F. E. *J. Mol. Catal. A: Chem.* **2010**, *331*, 117.

(4) (a) Fronczek, F. R.; Luck, R. L.; Wang, G. *Inorg. Chim. Acta* **2003**, *342*, 247. (b) Hursthouse, M. B.; Levason, W.; Ratnani, R.; Reid, G. *Polyhedron* **2004**, *23*, 1915. (c) Jimtaisong, A.; Luck, R. L. *Inorg. Chem.* **2006**, *45*, 10391.

(5) (a) Davis, M. F.; Levason, W.; Light, M. E.; Ratnani, R.; Reid, G.; Saraswat, K.; Webster, M. *Eur. J. Inorg. Chem.* **2007**, 1903. (b) Brown, M. D.; Hursthouse, M. B.; Levason, W.; Ratnani, R.; Reid, G. *Dalton Trans.* **2004**, 2487.

(6) (a) Arzoumanian, H.; Bakhtchadjian, R.; Agrifoglio, G.; Atencio, R.; Briceño, A. *Transition Met. Chem.* **2006**, *31*, 681. (b) Pereira, C. C. L.; Balula, S. S.; Paz, F. A. A.; Valente, A. A.; Pillinger, M.; Klinowski, J.; Gonçalves, I. S. *Inorg. Chem.* **2007**, *46*, 8508. (c) Coelho, A. C.; Nolasco, M.; Balula, S. S.; Antunes, M. M.; Pereira, C. C. L.; Paz, F. A. A.; Valente, A. A.; Pillinger, M.; Ribeiro-Claro, P.; Klinowski, J.; Gonçalves, I. S. *Inorg. Chem.* **2011**, *50*, 525. (d) Amarante, T. R.;

Gomes, A. C.; Neves, P.; Paz, F. A. A.; Valente, A. A.; Pillinger, M.; Gonçalves, I. S. *Inorg. Chem. Commun.* **2013**, *32*, 59.
(7) Levason, W.; Ratnani, R.; Reid, G.; Webster, M. *Inorg. Chim. Acta* **2006**, *359*, 4627.
(8) Amarante, T. R.; Neves, P.; Tomé, C.; Abrantes, M.; Valente, A. A.; Paz, F. A. A.; Pillinger, M.; Gonçalves, I. S. *Inorg. Chem.* **2012**, *51*, 3666.
(9) Abrantes, M.; Amarante, T. R.; Antunes, M. M.; Gago, S.; Paz, F. A. A.; Margiolaki, I.; Rodrigues, A. E.; Pillinger, M.; Valente, A. A.; Gonçalves, I. S. *Inorg. Chem.* **2010**, *49*, 6865.
(10) Figueiredo, S.; Gomes, A. C.; Neves, P.; Amarante, T. R.; Paz, F. A. A.; Soares, R.; Lopes, A. D.; Valente, A. A.; Pillinger, M.; Gonçalves, I. S. *Inorg. Chem.* **2012**, *51*, 8629.
(11) (a) Hagrman, P. J.; Hagrman, D.; Zubieta, J. *Angew. Chem., Int. Ed.* **1999**, *38*, 2638. (b) Hagrman, D.; Hagrman, P. J.; Zubieta, J. *Comments Inorg. Chem.* **1999**, *21*, 225. (c) Han, W.; Yuan, P.; Fan, Y.; Liu, H.; Bao, X. *J. Mater. Chem.* **2012**, *22*, 12121. (d) Han, W.; Yuan, P.; Fan, Y.; Shi, G.; Liu, H.; Bai, D.; Bao, X. *J. Mater. Chem.* **2012**, *22*, 25340. (e) Amarante, T. R.; Neves, P.; Valente, A. A.; Paz, F. A. A.; Fitch, A. N.; Pillinger, M.; Gonçalves, I. S. *Inorg. Chem.* **2013**, *52*, 4618 and references cited therein.
(12) (a) Thiel, W. R.; Angstl, M.; Priermeier, T. *Ber. Bunsen-Ges.* **1994**, *127*, 2373. (b) Thiel, W. R.; Priermeier, T. *Angew. Chem., Int. Ed. Engl.* **1995**, *34*, 1737. (c) Hinner, M. J.; Grosche, M.; Herdtweck, E.; Thiel, W. R. *Z. Anorg. Allg. Chem.* **2003**, *629*, 2251. (d) Bruno, S. M.; Pereira, C. C. L.; Balula, M. S.; Nolasco, M.; Valente, A. A.; Hazell, A.; Pillinger, M.; Ribeiro-Claro, P.; Gonçalves, I. S. *J. Mol. Catal. A: Chem.* **2007**, *261*, 79. (e) Neves, P.; Amarante, T. R.; Gomes, A. C.; Coelho, A. C.; Gago, S.; Pillinger, M.; Gonçalves, I. S.; Silva, C. M.; Valente, A. A. *Appl. Catal., A* **2011**, *395*, 71.
(13) Brunner, H.; Scheck, T. *Ber. Bunsen-Ges.* **1992**, *125*, 701.
(14) Li, D. C.; Liu, Y.; Wei, P. H.; Hu, B.; Zhang, X. T. *Acta Crystallogr., Sect. E: Struct Rep. Online* **2009**, *65*, m1074.
(15) Frisch, M. J.; Trucks, G. W.; Schlegel, H. B.; Scuseria, G. E.; Robb, M. A.; Cheeseman, J. R.; Montgomery, Jr., J. A.; Vreven, T.; Kudin, K. N.; Burant, J. C.; Millam, J. M.; Iyengar, S. S.; Tomasi, J.; Barone, V.; Mennucci, B.; Cossi, M.; Scalmani, G.; Rega, N.; Petersson, G. A.; Nakatsuji, H.; Hada, M.; Ehara, M.; Toyota, K.; Fukuda, R.; Hasegawa, J.; Ishida, M.; Nakajima, T.; Honda, Y.; Kitao, O.; Nakai, H.; Klene, M.; Li, X.; Knox, J. E.; Hratchian, H. P.; Cross, J. B.; Bakken, V.; Adamo, C.; Jaramillo, J.; Gomperts, R.; Stratmann, R. E.; Yazyev, O.; Austin, A. J.; Cammi, R.; Pomelli, C.; Ochterski, J. W.; Ayala, P. Y.; Morokuma, K.; Voth, G. A.; Salvador, P.; Dannenberg, J. J.; Zakrzewski, V. G.; Dapprich, S.; Daniels, A. D.; Strain, M. C.; Farkas, O.; Malick, D. K.; Rabuck, A. D.; Raghavachari, K.; Foresman, J. B.; Ortiz, J. V.; Cui, Q.; Baboul, A. G.; Clifford, S.; Cioslowski, J.; Stefanov, B. B.; Liu, G.; Liashenko, A.; Piskorz, P.; Komaromi, I.; Martin, R. L.; Fox, D. J.; Keith, T.; Al-Laham, M. A.; Peng, C. Y.; Nanayakkara, A.; Challacombe, M.; Gill, P. M. W.; Johnson, B.; Chen, W.; Wong, M. W.; Gonzalez, C.; Pople, J. A.; *Gaussian 03,* Revision B.04; Gaussian, Inc., Wallingford, CT, 2003.
(16) Johnson III, R. D. (Ed.). NIST Computational Chemistry Comparison and Benchmark Database, NIST Standard Reference Database Number 101, Release 12. http://srdata.nist.gov/cccbdb (Aug 2005).
(17) Gomes, A. C.; Neves, P.; Figueiredo, S.; Fernandes, J. A.; Valente, A. A.; Paz, F. A. A.; Pillinger, M.; Lopes, A. D.; Gonçalves, I. S. *J. Mol. Catal. A: Chem.* **2013**, *370*, 64.
(18) Baur, W. H. *Acta Crystallogr., Sect.B: Struct. Sci.* **1974**, *30*, 1195.
(19) Zapf, P. J.; Haushalter, R. C.; Zubieta, J. *Chem. Mater.* **1997**, *9*, 2019.
(20) Grell, J.; Bernstein, J.; Tinhofer, G. *Acta Crystallogr., Sect.B: Struct. Sci.* **1999**, *55*, 1030.
(21) Lu, Y.; Wang, E.; Yuan, M.; Li, Y.; Hu, C. *J. Mol. Struct.* **2003**, *649*, 191.
(22) Kim, J.; Lim, W. T.; Koo, B. K. *Inorg. Chim. Acta* **2007**, *360*, 2187.
(23) Zhao, B.; Chen, X.-Y.; Cheng, P.; Ding, B.; Liao, D.-Z.; Yan, S.-P.; Jiang, Z.-H. *J. Coord. Chem.* **2005**, *58*, 467.
(24) Zhou, D. P.; Bi, D. Q. *Z. Kristallogr.—New Cryst. Struct.* **2006**, *221*, 503.
(25) Zhou, Y.; Zhang, L.; Fun, H.-K.; You, X. *Inorg. Chem. Commun.* **2000**, *3*, 114.
(26) Dai, L.-M.; You, W.-S.; Li, Y.-G.; Wang, E.-B.; Qi, L.-J.; Tang, J.; Bai, X.-L. *Inorg. Chem. Commun.* **2010**, *13*, 421.
(27) Li, Y.-G.; Dai, L.-M.; Wang, Y.-H.; Wang, X.-L.; Wang, E.-B.; Su, Z.-M.; Xu, L. *Chem. Commun.* **2007**, 2593.
(28) (a) Allen, F. H. *Acta Crystallogr., Sect. B: Struct. Sci.* **2002**, *58*, 380. (b) Allen, F. H.; Motherwell, W. D. S. *Acta Crystallogr., Sect. B: Struct. Sci.* **2002**, *58*, 407.
(29) (a) Figueiredo, S.; Gomes, A. C.; Fernandes, J. A.; Paz, F. A. A.; Lopes, A. D.; Lourenço, J. P.; Pillinger, M.; Gonçalves, I. S. *J. Organomet. Chem.* **2013**, *723*, 56. (b) Amarante, T. R.; Paz, F. A. A.; Gago, S.; Gonçalves, I. S.; Pillinger, M.; Rodrigues, A. E.; Abrantes, M. *Molecules* **2009**, *14*, 3610. (c) Carreiro, E. P.; Yong-En, G.; Burke, A. J. *Inorg. Chim. Acta* **2006**, *359*, 1519. (d) Brito, J. A.; Gómez, M.; Muller, G.; Teruel, H.; Clinet, J. C.; Duñach, E.; Maestro, M. A. *Eur. J. Inorg. Chem.* **2004**, 4278. (e) Glas, H.; Spiegler, M.; Thiel, W. R. *Eur. J. Inorg. Chem.* **1998**, 275. (f) Herrmann, W. A.; Thiel, W. R.; Kuchler, J. G.; Behm, J.; Herdtweck, E. *Ber. Bunsen-Ges.* **1990**, *123*, 1963. (g) Schlemper, E. O.; Schrauzer, G. N.; Hughes, L. A. *Polyhedron* **1984**, *3*, 377.
(30) Amarante, T. R.; Neves, P.; Coelho, A. C.; Gago, S.; Valente, A. A.; Paz, F. A. A.; Pillinger, M.; Gonçalves, I. S. *Organometallics* **2010**, *29*, 883.
(31) Twu, J.; Fang, T. H.; Hsu, C. F.; Yu, Y. Y.; Wang, G. J.; Tang, C. W.; Chen, K. H.; Lii, K. H. *J. Mater. Chem.* **1998**, *8*, 2181.
(32) Griffith, W. P. *J. Chem. Soc. A* **1969**, 211.
(33) (a) Arzoumanian, H.; Bakhtchadjian, R.; Agrifoglio, G.; Krentzien, H.; Daran, J. C. *Eur. J. Inorg. Chem.* **1999**, 2255. (b) Monteiro, B.; Gago, S.; Neves, P.; Valente, A. A.; Gonçalves, I. S.; Pereira, C. C. L.; Silva, C. M.; Pillinger, M. *Catal. Lett.* **2009**, *129*, 350.
(34) Sanchez, C.; Belleville, P.; Popall, M.; Nicole, L. *Chem. Soc. Rev.* **2011**, *40*, 696.